2008

As particles collide: Extra dimensions and heavy leptons

Erin Kathleen De Pree
College of William & Mary - Arts & Sciences

As Particles Collide: Extra Dimensions and Heavy Leptons

Erin Kathleen De Pree

Midland, Michigan

Masters of Science, The College of William and Mary, 2004
Bachelors of Science, Hillsdale College, 2003

A Dissertation presented to the Graduate Faculty
of the College of William and Mary in Candidacy for the Degree of
Doctor of Philosophy

Department of Physics

The College of William and Mary
August 2008

APPROVAL PAGE

This dissertation is submitted in partial fulfillment of
the requirements for the degree of

Doctor of Philosophy

Erin Kathleen De Pree

Approved by the Committee, June 2008

Committee Chair
Professor Marc Sher, Physics
The College of William and Mary

Associate Professor Christopher Carone, Physics
The College of William and Mary

Assistant Professor Joshua Erlich, Physics
The College of William and Mary

Assistant Professor Jeffrey Nelson, Physics
The College of William and Mary

Associate Professor Deonna Woolard, Physics
Randolph-Macon College

ABSTRACT PAGE

Despite excellent agreement with experiment, the Standard Model leaves several issues unresolved. These issues will be explored and several extensions to the Standard Model introduced: models with extra dimensions and a fourth family of particles.

In extra dimensional models, there are Fourier modes of the Standard Model particles. We study the detection of bound states of one of the modes and its Standard Model particle.

We then explore a particular model of extra dimensions known as Randall-Sundrum or warped extra dimensions. We will see how this model affects top quark measurements at the proposed International Linear Collider.

Finally we will study the detection of heavy charged leptons at both the Large Hadron and International Linear Colliders.

Contents

List of Figures

List of Tables

Dedication

In honor of my students: former and future

Acknowledgments

There have been many people who have made finishing graduate school possible. My deepest gratitude to the following:

- My parents – Paul and Kathy – for their love and encouragement.
- My siblings – Joanna, Heather, Kelsey, and Kurtis – for their unwavering love and reminders that life continues outside of grad school.
- My advisor, Marc Sher
- Ken Hayes, my undergraduate advisor at Hillsdale College. His ability to challenge and encourage his students is one I wish emulate.
- Deonna Woodard, Department Chair of Physics at Randolph-Macon College in Ashland, Virginia, who gave me a job teaching "A Hitchhiker's Guide to Physics" and then let me develop my own course. Teaching that class changed my life.
- All my friends in Quarters – I love you all and will miss you.
- Sebastian – my fuzzy cat who supervised me while I was writing this dissertation, except he slept the entire time! Don't worry, there's tuna fish in Maryland too.

To the numerous people who have touched my life and helped me to grow in many ways as a person during my time in Williamsburg – thank you.

Chapter 1

Introduction

Elementary particle physics is the study of the fundamental particles in nature. These are particles without internal structure. For example, the electron is a fundamental particle, while the proton, consisting of quarks and gluons, is not.

Fundamental particles are studied in particle accelerators or colliders, which accelerate them to very high energies. Detectors observe the results when two groups of particles smash together. As the energy of the particles increases, we are able to see interactions at smaller distance scales.

The current description of the fundamental particles and their interactions is the Standard Model (SM). It consists of 12 fundamental fermions – particles with half-integral spin – subjected to three interactions: electromagnetic, weak, and strong. The Standard Model does not include the gravitational interaction. Initially formulated in the 1970s [1, 2, 3], the Standard Model has been extremely successful in its predictions and tests.

However, there are unanswered questions in the theory, which prompted

the eager particle theory community to propose a vast and diverse collection of possible theories or models to replace or extend the Standard Model. Because of the experimental success of the Standard Model, the new theories must reduce to (or replicate) the Standard Model at low energies. Essentially we are searching for a new theory that explains physics at energies above about 1 TeV. Any ideas building upon the Standard Model are referred to as *Physics Beyond the Standard Model.*

New theories have taken on new life as time approaches for the Large Hadron Collider (LHC) to turn on (currently predicted to be late 2008). With a center-of-mass energy of 14 TeV, the LHC is expected to reveal new physics in the near future. Additionally an electron-positron collider, the International Linear Collider (ILC), is currently being planned, however it will not turn on for at least another decade.

A major challenge – after collecting the data which alone presents a significant challenge – of these new experiments is analyzing the data and searching for the existence of any new particles or new decay modes, etc. It is here that high-energy phenomenology steps in. The phenomenology of a theory explains what new signatures to expect in a detector. By noting the presence or absence of a particular signature, it is possible to determine whether a theory has been excluded or not by the new data.

There are many theories, each with a myriad of variations, to consider. This dissertation studies some variations of two theories – extra dimensions and heavy leptons – and explores distinguishing signatures to set them apart from the Standard Model and competing alternatives.

This dissertation will review the Standard Model in Chapter 2 before discussing several extensions to the Standard Model. We focus first on the addition of an extra spatial dimension. "Rolling up" the extra dimension leads to the existence of progressively heavier copies of particles or Fourier modes, called Kaluza-Klein (KK) particles. These new particles create new decay signatures to detect. The second extension to the Standard Model is the existence of a fourth generation of matter.

In Chapter 3, we will study how to detect a signature of KK mesons, made of a KK quark and a regular Standard Model quark. Many models, such as supersymmetric models, have long-lived "copies" of Standard Model particles. The bound states of two of these "copies" have been studied, while mesons of one "copy" and a Standard Model quark have not.

Chapter 4 will focus on a particular model of extra dimensions known as Randall-Sundrum or warped extra dimensions. We will see how this model affects top quark measurements at the proposed ILC.

The focus shifts in Chapter 5 with the addition of a fourth generation to the

Standard Model. Our analysis will include detecting the heavy charged leptons at both the upcoming LHC and the proposed ILC. Finally, our summary and conclusions will be presented in Chapter 6.

Chapter 2

Standard Model and Beyond

In this Chapter, we discuss the Standard Model (SM): the theoretical foundation, experimental evidence, shortcomings, and two interesting extensions of the SM.

2.1 Theory

The currently accepted description of the types of particles and how they interact – called the Standard Model – was initially developed in the 1970s[1]. It divides all spin-1/2 particles, or fermions, into three families, or generations, of matter. Each family consists of two quarks and two leptons. Table 2.1 displays

[1]Foundational papers include Ref. [1, 2, 3]. This chapter will introduce parts of the Standard Model necessary for this the dissertation. A complete overview of the Standard Model can be found in Ref. [4].

all twelve of the Standard Model particles [4].

Particle	Flavor			$Q/\|e\|$
leptons	e	μ	τ	-1
	ν_e	ν_μ	ν_τ	0
quarks	u	c	t	$+\frac{2}{3}$
	d	s	b	$-\frac{1}{3}$

Table 2.1: The fundamental fermions

These particles are subjected to four types of interactions, three of which are described by the Standard Model. The Standard Model does not include the gravitational interaction which is many orders of magnitude weaker than the electromagnetic, weak, and strong interactions. These interactions are described by the gauge group $\mathrm{SU}(3)_C \times \mathrm{SU}(2)_L \times \mathrm{U}(1)_Y$.

$\mathrm{SU}(3)_C$ describes the strong interaction; a theory known as *Quantum Chromodynamics* (QCD). Just as electromagnetism only affects charged fermions, the strong interaction only affects particles with color – quarks. While electromagnetism has two charges – positive or negative, the strong interaction has three colors – red, green, and blue. These are not actual visible colors, but a useful way of distinguishing the three "charges" of the strong interaction. QCD will be further discussed in Subsection 2.1.4.

The next sections will be devoted to the standard electroweak theory given by $\mathrm{SU}(2)_L \times \mathrm{U}(1)_Y$.

2.1.1 Electroweak Interaction – $SU(2) \times U(1)$

The electroweak interaction in the Standard Model is based on an $SU(2)_L \times U(1)_Y$ gauge theory. Eventually the $SU(2)_L \times U(1)_Y$ group needs to break to $U(1)_{\mathrm{EM}}$, the electromagnetic interaction. The charges of the new group $SU(2)_L \times U(1)_Y$ are the weak charges, T_+, T_-, and T_3, for $SU(2)_L$ and the hypercharge, Y, for $U(1)_Y$. The hypercharge Y of a particle depends on both T_3 and the electric charge Q as follows:

$$Y = 2(Q - T_3). \tag{2.1}$$

Fermions are left-handed doublets and right-handed singlets. The electroweak Lagranian is

$$\mathcal{L} = \mathcal{L}_{\mathrm{gauge}} + \mathcal{L}_{\mathrm{fermion}} + \mathcal{L}_{\mathrm{Higgs}} + \mathcal{L}_{\mathrm{Yukawa}}. \tag{2.2}$$

We will now discuss each contribution to the Lagrangian.

Gauge Fields

We begin with the gauge fields for $SU(2)$ and $U(1)$: an isotriplet $\mathbf{W}_\mu$ for $\mathrm{SU}(2)_L$ and a singlet B_μ for $\mathrm{U}(1)_Y$. The gauge Lagrangian density is

$$\mathcal{L}_{\mathrm{gauge}} = -\frac{1}{4}\mathbf{W}^{\mu\nu}\mathbf{W}_{\mu\nu} - \frac{1}{4}B^{\mu\nu}B_{\mu\nu} \tag{2.3}$$

where

$$B_{\mu\nu} = \partial_\mu B_\nu - \partial_\nu B_\mu \tag{2.4}$$

and

$$W^i_{\mu\nu} = \partial_\mu W^i_\nu - \partial_\nu W^i_\mu - g f^{ijk} W^j_\mu W^k_\nu \tag{2.5}$$

where $i, j, k = 1, 2, 3$, g is the weak coupling coupling constant, and f^{ijk} is the structure constant. This gives four gauge bosons: B_μ, W^1_μ, W^2_μ, and W^3_μ. The gauge symmetry forbids mass terms, so the gauge bosons are massless.

Fermions

Next we add fermions ψ. There are left-handed doublets

$$l_L = \begin{pmatrix} \nu_L \\ e_L \end{pmatrix} \quad \text{and} \quad q_L = \begin{pmatrix} u_L \\ d_L \end{pmatrix} \tag{2.6}$$

and right-handed singlets: e_R, u_R, and d_R. For simplicity, we have suppressed the family number. The gauge invariant Lagrangian for fermions is

$$\mathcal{L}_{\text{fermion}} = \bar{\psi} i \gamma^\mu D_\mu \psi. \tag{2.7}$$

γ^μ are the Dirac matrices and

$$D_\mu \psi = \left(\partial_\mu - i\frac{g}{2}\boldsymbol{\sigma} \cdot \mathbf{W}_\mu - ig'\frac{Y}{2}B_\mu \right) \psi \tag{2.8}$$

where σ^i are the Pauli matrices, and g' is the B field coupling constant. The hypercharges for the fermions are

$$Y(l_L) = -1, \qquad Y(e_R) = -2,$$

$$Y(q_L) = 1/3, \qquad Y(u_R) = 4/3, \quad \text{and} \quad Y(d_R) = -2/3. \tag{2.9}$$

For example:

$$D_\mu l_L = \left(\partial_\mu - \frac{g}{2}\boldsymbol{\sigma} \cdot \mathbf{W}_\mu - i\frac{g'}{2}B_\mu \right) l_L \tag{2.10}$$

$$D_\mu e_R = \left(\partial_\mu + ig'B_\mu \right) e_R \tag{2.11}$$

The W boson only acts on left-handed particles. Further, the Lagrangian does not include any fermion mass terms. So at this point we only have massless particles – clearly not what we have in nature.

Massive gauge bosons

Mass terms for gauge bosons are not gauge invariant. The only renormalizable mechanism for giving the gauge bosons mass is the Higgs mechanism.

We introduce a complex scalar doublet

$$\Phi = \begin{pmatrix} \phi^+ \\ \phi^0 \end{pmatrix}, \qquad Y_\Phi = 1 \tag{2.12}$$

to break the symmetry. Its Lagrangian density is

$$\mathcal{L}_\Phi = (D_\mu \Phi)^\dagger (D^\mu \Phi) - \mu^2 \Phi^\dagger \Phi - \lambda \left(\Phi^\dagger \Phi\right)^2 \tag{2.13}$$

with $\lambda > 0$ and $\mu^2 < 0$. Gauge invariance is assured if

$$D^\mu = \partial^\mu - \frac{i}{2} g \boldsymbol{\sigma} \cdot \mathbf{W}^\mu - \frac{i}{2} g' Y_\Phi B^\mu. \tag{2.14}$$

The scalar field Φ is also coupled to the fermions. This will eventually give the fermions mass. The coupling terms, suppressing family indices, are

$$\mathcal{L}_{\text{Yukawa}} = f^{(e)} \bar{l}_L \Phi e_R + f^{(u)} \bar{q}_L \tilde{\Phi} u_R + f^{(d)} \bar{q}_L \Phi d_R + \text{h.c.} \tag{2.15}$$

where $\tilde{\Phi} = i\tau_L \Phi^*$ with hypercharge $Y_{\tilde{\Phi}} = -1$ and h.c. means Hermitian conju-

gate.

In Subsection 2.1.3, spontaneous symmetry will be discussed in detail. For now, in the unitary gauge, the vacuum expectation value of Φ is

$$\langle \Phi \rangle_0 \equiv \begin{pmatrix} 0 \\ v/\sqrt{2} \end{pmatrix}, \tag{2.16}$$

where $v = \sqrt{-\mu^2/\lambda}$. Expanding the scalar field about the vacuum state, we obtain

$$\Phi(x) = \begin{pmatrix} 0 \\ \frac{v+\eta(x)}{\sqrt{2}} \end{pmatrix} = \frac{v + \eta(x)}{\sqrt{2}} \chi, \tag{2.17}$$

where $\chi = \begin{pmatrix} 0 \\ 1 \end{pmatrix}$. $\mathcal{L}_\Phi$ is rewritten as

$$\mathcal{L}_\Phi = (D_\mu \Phi)^\dagger (D^\mu \Phi) - \mu^2 \eta^2 - \lambda v \eta^3 - \frac{\lambda}{4} \eta^4. \tag{2.18}$$

We next rewrite the Yukawa Lagrangian:

$$\begin{aligned} \mathcal{L}_{\text{Yukawa}} =& \frac{\eta(x)}{\sqrt{2}} \left(f^{(e)} \bar{e}_L e_R + f^{(u)} \bar{u}_L u_R + f^{(d)} \bar{d}_L d_R \right) \\ &+ \frac{v}{\sqrt{2}} \left(f^{(e)} \bar{e}_L e_R + f^{(u)} \bar{u}_L u_R + f^{(d)} \bar{d}_L d_R \right) + \text{h.c.} \end{aligned} \tag{2.19}$$

Mass Spectrum

Now that we have rewritten the Lagrangian, we can read off the masses. The mass of the scalar field η is

$$m_\eta^2 = 2\lambda v^2. \tag{2.20}$$

η is the neutral Higgs.

The fermion masses, which depend on their Yukawa couplings f and the vacuum expectation value v, are

$$\begin{aligned} m_e &= f^{(e)} v/\sqrt{2}, \\ m_u = f^{(u)} v/\sqrt{2}, \quad &\text{and} \quad m_d = f^{(d)} v/\sqrt{2}. \end{aligned} \tag{2.21}$$

The vector mesons receive masses from the kinetic term. The derivative independent parts of the $(D_\mu \Phi)^\dagger (D^\mu \Phi)$ term give

$$\begin{aligned} &\frac{v^2}{2} \chi^\dagger \left(\frac{g}{2} \boldsymbol{\tau} \cdot \mathbf{W}_\mu + \frac{g'}{2} B_\mu \right) \left(\frac{g}{2} \boldsymbol{\tau} \cdot \mathbf{W}_\mu + \frac{g'}{2} B_\mu \right) \chi \\ &= \frac{v^2}{8} \left(g^2 \left[(W_\mu^1)^2 + (W_\mu^2)^2 \right] + \left[g W_\mu^3 - g' B_\mu \right]^2 \right) \\ &= M_W^2 W_\mu^+ W^{\mu -} + \frac{1}{2} M_Z^2 Z_\mu Z^\mu \end{aligned} \tag{2.22}$$

where

$$W_\mu^\pm = \frac{1}{\sqrt{2}} \left(W_\mu^1 \mp i W_\mu^2 \right). \tag{2.23}$$

From this we can see that the mass of the $W^{\pm}$ boson is given by

$$M_W^2 = \frac{g^2 v^2}{4}. \tag{2.24}$$

The new neutral fields W_μ^3 and B_μ mix together form the Z and the photon:

$$\begin{aligned}
\frac{1}{2} M_Z^2 Z_\mu Z^\mu &= \frac{v^2}{8} \left(g W_\mu'^3 - g' B_\mu' \right)^2 \\
&= \frac{v^2}{8} \begin{pmatrix} W_\mu'^3 & B_\mu' \end{pmatrix} \begin{pmatrix} g^2 & -gg' \\ -gg' & g'^2 \end{pmatrix} \begin{pmatrix} W'^{3\mu} \\ B'^{\mu} \end{pmatrix} \\
&= \frac{1}{2} \begin{pmatrix} Z_\mu & A_\mu \end{pmatrix} \begin{pmatrix} M_Z^2 & 0 \\ 0 & 0 \end{pmatrix} \begin{pmatrix} Z^\mu \\ A^\mu \end{pmatrix}
\end{aligned} \tag{2.25}$$

where

$$\begin{aligned}
Z_\mu &= \cos\theta_W W_\mu'^3 - \sin\theta_W B_\mu' \\
A_\mu &= \sin\theta_W W_\mu'^3 + \cos\theta_W B_\mu'
\end{aligned} \tag{2.26}$$

with

$$\tan\theta_W = g'/g. \tag{2.27}$$

The mass of the Z boson is given by

$$M_Z^2 = \frac{v^2}{4}\left(g^2 + g'^2\right) \tag{2.28}$$

and the photon is massless. We now rewrite the fermion-gauge coupling terms of Eq. (2.7) in terms of currents:

$$\begin{aligned}
&\bar{l}_L\gamma^\mu\left[\frac{g}{2}\boldsymbol{\tau}\cdot\mathbf{W}_\mu - \frac{g'}{2}B_\mu\right]l_L + \bar{q}_L\gamma^\mu\left[\frac{g}{2}\boldsymbol{\tau}\cdot\mathbf{W}_\mu + \frac{g'}{6}B_\mu\right]q_L \\
&\quad + \bar{e}_R\gamma^\mu\left[-g'B_\mu\right]e_R + \bar{u}_R\gamma^\mu\left[\frac{2g'}{3}B_\mu\right]u_R + \bar{d}_R\gamma^\mu\left[-\frac{g'}{3}B_\mu\right]d_R \\
&= g\left(\frac{1}{2}\bar{l}_L\boldsymbol{\tau}\gamma^\mu l_L + \frac{1}{2}\bar{q}_L\boldsymbol{\tau}\gamma^\mu q_L\right)\mathbf{W}_\mu \\
&\quad + g'\left(-\frac{1}{2}\bar{l}_L\boldsymbol{\tau}\gamma^\mu l_L + \frac{1}{6}\bar{q}_L\boldsymbol{\tau}\gamma^\mu q_L - \bar{e}_R\boldsymbol{\tau}\gamma^\mu e_R + \frac{2}{3}\bar{u}_R\boldsymbol{\tau}\gamma^\mu u_R - \frac{1}{3}\bar{d}_R\boldsymbol{\tau}\gamma^\mu d_R\right)B_\mu \\
&\equiv \left(gJ^{1\mu}W_\mu^1 + gJ^{2\mu}W_\mu^2\right) + \left(gJ^{3\mu}W_\mu^3 + g'J^{Y\mu}B\mu\right).
\end{aligned} \tag{2.29}$$

We observe that the terms can be rewritten in terms of a charged and neutral current.

The charged current is given by

$$\begin{aligned}
J_\mu^1 &= \frac{1}{2}\left(\bar{\nu}_L\gamma_\mu e_L + \bar{e}_L\gamma_\mu\nu_L + \bar{u}_L\gamma_\mu d_L + \bar{d}_L\gamma_\mu u_L\right) \\
J_\mu^2 &= \frac{i}{2}\left(-\bar{\nu}_L\gamma_\mu e_L + \bar{e}_L\gamma_\mu\nu_L - \bar{u}_L\gamma_\mu d_L + \bar{d}_L\gamma_\mu u_L\right).
\end{aligned} \tag{2.30}$$

These currents can be linearly combined into positive and negative currents given by

$$\begin{aligned} J_\mu^+ &= J_\mu^1 + iJ_\mu^2 \\ &= \bar{\nu}_L \gamma_\mu e_L + \bar{u}_L \gamma_\mu d_L \\ &= \frac{1}{2}\bar{\nu}\gamma_\mu(1-\gamma_5)e + \frac{1}{2}\bar{u}\gamma_\mu(1-\gamma_5)d \end{aligned} \tag{2.31}$$

and

$$\begin{aligned} J_\mu^- &= J_\mu^1 - iJ_\mu^2 \\ &= \bar{e}_L \gamma_\mu \nu_L + \bar{d}_L \gamma_\mu u_L \\ &= \frac{1}{2}\bar{e}\gamma_\mu(1-\gamma_5)\nu + \frac{1}{2}\bar{d}\gamma_\mu(1-\gamma_5)u. \end{aligned} \tag{2.32}$$

The charged current Lagrangian is then given by

$$\begin{aligned} \mathcal{L}_{\mathrm{CC}} &= \left(gJ_\mu^1 W^{1\mu} + gJ_\mu^2 W^{2\mu}\right) \\ &= \frac{g}{\sqrt{2}}\left(J_\mu^+ W^{+\mu} + J_\mu^- W^{-\mu}\right). \end{aligned} \tag{2.33}$$

At low energies this interaction is written as an effective Lagrangian, given by

$$\mathcal{L}_{\mathrm{eff}}^{\mathrm{CC}} = -\frac{g^2}{2M_W^2} J_\mu^+ J^{-\mu}. \tag{2.34}$$

The Fermi theory described β-decay $d_L \rightarrow u_L\, e_L\, \bar{\nu}_R$ as a vector-minus-axial-vector (V–A) coupling. The Lagrangian describing the Fermi theory is

$$\mathcal{L}_F = -\frac{G_F}{\sqrt{2}}\left[\bar{u}(x)\gamma_\mu \frac{1}{2}(1-\gamma_5)d(x)\right]\left[\bar{e}(x)\gamma^\mu \frac{1}{2}(1-\gamma_5)\nu(x)\right] + \text{h.c.} \tag{2.35}$$

where G_F is the Fermi coupling constant, given by

$$G_F \simeq \frac{10^{-5}}{m_p^2}. \tag{2.36}$$

The four fermion interaction can be rewritten in terms of the weak current as given by

$$\mathcal{L}_F = -\frac{G_F}{\sqrt{2}} J_\mu^\dagger(x) J^\mu(x) + \text{h.c.} \tag{2.37}$$

Comparing Eqs. (2.34) and (2.37), it is clear that at low energies the weak charged current interactions can be modeled as an interaction between four fermions. After accounting for the extra factor of $\frac{1}{2}$ in the charged currents, we can easily see that

$$\frac{G_F}{\sqrt{2}} = \frac{g^2}{8M_W^2}. \tag{2.38}$$

Using Eq. (2.24), we expect a vacuum expectation value on the order of

$$v = 2^{-1/4} G_F^{-1/2} \simeq 250\,\text{GeV}. \tag{2.39}$$

2.1.2 Spontaneous Symmetry Breaking

Global Symmetry Breaking

Consider a complex scalar field $\Phi = \frac{1}{\sqrt{2}}(\phi_1' + i\phi_2')$. The Lagrangian density is

$$\mathcal{L} = \partial_\mu \Phi^\dagger \partial^\mu \Phi - \mu^2 \Phi^\dagger \Phi - \lambda \left(\Phi^\dagger \Phi\right)^2. \tag{2.40}$$

If μ^2 is positive, the minimum state occurs when $\phi_1' = \phi_2' = 0$. If the sign in front of μ^2 is changed, the potential would be unstable at the origin. In that case, we can write

$$\mathcal{L} = \partial_\mu \Phi^\dagger \partial^\mu \Phi - V(\Phi^\dagger \Phi) \tag{2.41}$$

where

$$V(\Phi^\dagger \Phi) = \frac{\mu^2}{2v^2}\left[\Phi^\dagger \Phi - v^2\right]^2. \tag{2.42}$$

Now the minimum vacuum value is $v = \sqrt{-\mu^2/\lambda}$. This occurs not at a point, but a set of continuous vacuum states on a circle $|\Phi| = v$. Expanding about this ground state choosing $\phi_1' = v$ and $\phi_2' = 0$, we have $\Phi = v + \frac{1}{\sqrt{2}}(\phi_1 + i\phi_2)$. Since v is a constant, $\partial_\mu v = 0$, the Lagrangian density becomes

$$\mathcal{L} = \frac{1}{2}\partial_\mu \phi_1 \partial^\mu \phi_1 + \frac{1}{2}\partial_\mu \phi_2 \partial^\mu \phi_2 - \frac{\mu^2}{2v^2}\left(\sqrt{2}v\phi_1 + \frac{\phi_1^2}{2} + \frac{\phi_2^2}{2}\right)^2. \tag{2.43}$$

Having broken the $U(1)$ symmetry, instead of one complex field Φ, now we have two coupled real scalar fields ϕ_1 and ϕ_2 [5]. ϕ_1 is a scalar of mass $\sqrt{2\lambda}v$, while ϕ_2 is a massless spin-zero particle called a Goldstone boson. Goldstone bosons always appear when a global symmetry is broken.

Local Symmetry Breaking

Consider a complex scalar field Φ and a $U(1)$ gauge field B_μ.

$$\mathcal{L} = (D_\mu\Phi)(D^\mu\Phi) - \mu^2\Phi^\dagger\Phi - \lambda(\Phi^\dagger\Phi)^2 - \frac{1}{4}F_{\mu\nu}F^{\mu\nu} \tag{2.44}$$

with

$$\begin{aligned} D_\mu\Phi &= (\partial_\mu - igB_\mu)\Phi \\ F_{\mu\nu} &= \partial_\mu B_\nu - \partial_\nu B_\mu. \end{aligned} \tag{2.45}$$

The Lagrangian is invariant under the local gauge transformation

$$\begin{aligned} \Phi(x) &\rightarrow \Phi' = e^{-i\alpha(x)}\Phi(x) \\ B_\mu(x) &\rightarrow B'_\mu(x) = B_\mu(x) - \frac{1}{g}\partial_\mu\alpha(x) \end{aligned} \tag{2.46}$$

for any $\alpha(x)$. Assuming $\mu^2 < 0$, the potential $V(\Phi) = \mu^2\Phi^\dagger\Phi + \lambda(\Phi^\dagger\Phi)^2$ is minimized at $|\Phi| = v/\sqrt{2}$ where $v = \sqrt{-\mu^2/\lambda}$. Φ develops a vacuum expectation

value

$$|\langle 0|\Phi|0\rangle| = v/\sqrt{2}. \tag{2.47}$$

We rewrite Φ in terms of two real fields ϕ_1' and ϕ_2'

$$\Phi = \frac{1}{\sqrt{2}}(\phi_1' + i\phi_2') \tag{2.48}$$

and choose

$$\langle 0|\phi_1'|0\rangle = v \qquad \text{and} \qquad \langle 0|\phi_2'|0\rangle = 0. \tag{2.49}$$

We shift the scalar fields

$$\phi_1 = \phi_1' - v \qquad \text{and} \qquad \phi_2 = \phi_2' \tag{2.50}$$

and rewrite the $|D_\mu\Phi|^2$ term

$$\begin{aligned} |D_\mu\Phi|^2 &= |(\partial_\mu - igB_\mu)\Phi|^2 \\ &= \frac{1}{2}(\partial_\mu\phi_1 + gB_\mu\phi_2)^2 + \frac{1}{2}(\partial_\mu\phi_2 - gB_\mu\phi_1)^2 \\ &\quad - gvB^\mu(\partial_\mu\phi_2 - gB_\mu\phi_1) + \frac{g^2v^2}{2}B_\mu B^\mu. \end{aligned} \tag{2.51}$$

The gauge field B_μ has acquired a mass $M = gv$. The term $-gvB^\mu\partial_\mu\phi_2$ allows the scalar field ϕ_2 and the gauge field B_μ to mix. In the next section we will

use gauge fixing to remove this mixing.

2.1.3 Gauge Fixing

We wish to remove the mixing term

$$-gvB^{\mu}\partial_{\mu}\phi_2 \tag{2.52}$$

from Eq. (2.51). In Eq. (2.46), we used $\alpha(x)$ to gauge transform both Φ and B_{μ}. One can choose $\alpha(x)$ such that

$$\partial^{\mu}B_{\mu} + \xi M\phi_2 = 0 \tag{2.53}$$

where ξ is an arbitrary parameter. This is implemented by including a delta function, $\delta(\partial^{\mu}B_{\mu} + \xi M\phi_2)$, in the path integral. This is equivalent to adding a gauge-fixing term,

$$\mathcal{L}_{\text{gf}} = -\frac{1}{2\xi}(\partial^{\mu}B_{\mu} + \xi M\phi_2)^2, \tag{2.54}$$

to the original Lagrangian. This eliminates the mixing term [6]:

$$\begin{aligned}\mathcal{L} = &\frac{1}{2}\left[(\partial^{\mu}\phi_1)^2 - 2\mu^2\phi_1^2\right] + \frac{1}{2}\left[(\partial^{\mu}\phi_2)^2 - \xi M^2\phi_2^2\right] \\ &- \frac{1}{4}(\partial_{\mu}B_{\nu} - \partial_{\nu}B_{\mu})^2 + \frac{1}{2}M^2B_{\mu}B^{\mu} - \frac{1}{2\xi}(\partial^{\mu}B_{\mu})^2.\end{aligned} \tag{2.55}$$

Propagator

Equation 2.55 yields three particles:

- Higgs scalar ϕ_1 with propagator

$$i\Delta_1(k) = \frac{i}{k^2 - 2\mu^2 + i\epsilon} \tag{2.56}$$

- Goldstone boson ϕ_2 with propagator

$$i\Delta_2(k) = \frac{i}{k^2 - \xi M^2 + i\epsilon} \tag{2.57}$$

- Gauge boson B_μ with propagator

$$i\Delta_{\mu\nu}(k) = \frac{-i}{k^2 - M^2 + i\epsilon}\left[g_{\mu\nu} - (1-\xi)\frac{k_\mu k_\nu}{k^2 - \xi M^2}\right] \tag{2.58}$$

These propagators are written in the R_ξ gauge. Since ξ is an arbitrary parameter, we can set it to whatever value is most convenient.

Feynman Gauge The Feynman gauge sets $\xi = 1$. This greatly simplifies calculations because the gauge boson propagator now has only one term. However the Goldstone boson ϕ_2 remains, leading to greater number of diagrams to calculate.

- Goldstone boson

$$\frac{-i}{k^2 - M^2 + i\epsilon} \tag{2.59}$$

- Gauge boson

$$\frac{ig_{\mu\nu}}{k^2 - M^2 + i\epsilon} \tag{2.60}$$

Unitary Gauge The Unitary gauge minimizes the number of fields by eliminating ϕ_2, the Goldstone bosons, by setting $\xi = \infty$. This comes at the price of complicating the gauge boson propagator

$$\frac{-i}{k^2 - M^2 + i\epsilon}\left[g_{\mu\nu} - \frac{k_\mu k_\nu}{M^2}\right] \tag{2.61}$$

Since all gauges are equivalent, the Unitary gauge is renormalizable, but it is much easier to renormalize other gauges.

Landau Gauge With $\xi = 0$, the Landau gauge is between the Feynman and Unitary gauges. Although both B_μ and ϕ_2 are present, the propagators are not complicated.

- Goldstone boson

$$\frac{i}{k^2 + i\epsilon} \tag{2.62}$$

- Gauge boson

$$\frac{-i}{k^2 - M^2 + i\epsilon}\left[g_{\mu\nu} - \frac{k_\mu k_\nu}{k^2}\right] \tag{2.63}$$

2.1.4 Strong Interaction – $SU(3)$

The fundamental difference between the strong interaction and the electroweak interaction is that the strong interaction is described by a non-Abelian group and acts only on quarks. The strong interaction Lagrangian:

$$\mathcal{L} = -\frac{1}{4}G_a^{\mu\nu}G_{a\mu\nu} + \bar{\psi}_j\left(i\gamma_\mu D_{jk}^\mu - M_{jk}\right)\psi_k \tag{2.64}$$

where M_{jk} is diagonal and the indices a, j, and k refer to color and have values $a = 1, \ldots, 8$, and $j, k = 1, 2, 3$. Further

$$D_{jk}^\mu = \delta_{jk}\partial^\mu + ig_s(T_a)_{jk}G_a^\mu \tag{2.65}$$

where G_a^μ are the gluon fields, T_a are the $SU(3)_C$ generators, and g_s is the strong coupling. M_{jk} is the quark mass matrix. The gluon field tensor $G_a^{\mu\nu}$ is

$$G_a^{\mu\nu} = \partial^\mu G_a^\nu - \partial^\nu G_a^\mu - g_s f_{abc}G_b^\mu G_c^\nu \tag{2.66}$$

where f_{abc} is a structure factor of $SU(3)_C$.

The three colors are traditionally called red, green, and blue. Each quark has a color charge, while each anti-quark has an anti-color. The quarks and anti-quarks are combined to created colorless particles: baryons, three quarks or three anti-quarks each of a different color, and mesons, a quark and anti-quark of the anti-color. Gluons are part of the octet representation of $SU(3)_C$. Gluons also carry a color charge: including red-antigreen or blue-antired and two linear combinations of red-antired, green-antigreen, and blue-antiblue. Gluons have no electrical charge or flavor; and as such are not subject to the electromagnetic or weak forces.

The combination of color charge and non-Abelian nature of the strong force lead to *asymptotic freedom*: at high energies, or short distances, the quarks act like free particles. This is the exact opposite of the electromagnetic force. The larger the separation between the quarks is the stronger the strong force between them.

2.2 Experimental Verification

Since the formulation of the Standard Model in the 1960s and 1970s, there have been many confirmations and verifications in a myriad of experiments. We will look at three significant confirmations of the Standard Model.

2.2.1 $W^{\pm}$ and Z Boson Mass Relationship

In 1983, the scientists at CERN's Super Proton Synchrotron (SPS) discovered the W and Z bosons within a few months of each other. In addition to the normal excitement of discovery, the mass of the Z boson covered the predicted range from the $SU(2)_L \times U(1)_Y$ electroweak theory. Given the mass of the W boson, the Z boson is set by the theory; the tree level value is

$$M_Z = \frac{M_W}{\cos\theta_W}. \tag{2.67}$$

This relationship was predicted by the Glashow-Weinberg-Salam (GWS) theory in the 1960s. The current Particle Data Group world average [7] for the Z mass is 91.1876 ± 0.0021 GeV; this predicts a W mass of 80.361 ± 0.020 GeV (this includes higher order corrections). The experimental measured W mass is 80.400 ± 0.024 GeV, in agreement with the predicted mass.

2.2.2 Top Quark

After the bottom quark was discovered in the late 1970s, a partner quark was needed to cancel anomalies and prevent unobserved flavor changing neutral currents. Further, as the first and second families of matter have two quarks and two leptons each, we expect the third family to follow the established pattern to preserve quark-lepton symmetry.

In 1995, the top quark was discovered by the DØ and CDF collaborations at Fermilab's $p\bar{p}$ Tevatron in Batavia, Illinois, United States. With a mass of 172.7 GeV, the top quark is over 30 times heavier than its weak-isospin partner, the bottom quark.

2.2.3 Precision Electroweak Measurements

The Standard Model excels in accurate predictions of precision electroweak measurements. With only five input values – the mass Z boson M_Z, the Fermi constant G_F, the fine structure constant α, the mass of the top quark m_t, and the mass of the Higgs m_H – many different observables can be calculated using the $SU(2)_L \times U(1)_Y$ electroweak theory and can also be independently measured. Even without knowing the Higgs mass, we can calculate the observables (although not as accurately).

The experimental and theoretical observable values overall agree to one part per thousand. See Table 2.2.3 for a list of electroweak precision observables from the Particle Data Group [7]. Although most experimental and theoretical values of the observables agree closely, a few differ enough to leave room for new physics.

The five parameters can be used to compare experimental and theoretical values. The experimental values can be used to limit the range of allowed

values for the parameters. For example, the directly measured top mass and the range allowed by the SM now agree very well. The unknown parameter – the Higgs mass – is also limited [7]:

$$m_H < 189 \text{ GeV}. \tag{2.68}$$

2.3 Problems

Despite its historic success, several problems have emerged that are not addressed by the Standard Model.

2.3.1 Gauge Hierarchy Problem

The scale of the weak interaction is ≈ 100 GeV. However the Grand Unified Theory and gravity scales are of the order 10^{16} GeV and 10^{19} GeV respectively. Thus to maintain the smallness of the weak scale requires canceling two large numbers almost exactly. This is called *fine-tuning* and does not adequately explain why the weak scale is so much smaller. This issue is the *Gauge Hierarchy Problem.*

Quantity	Value	Standard Model
m_t [GeV]	$172.7 \pm 2.9 \pm 0.6$	172.7 ± 2.8
M_W [GeV]	80.450 ± 0.058	80.376 ± 0.017
M_Z [GeV]	91.1876 ± 0.0021	91.1874 ± 0.0021
Γ_Z [GeV]	2.4952 ± 0.0023	2.4968 ± 0.0011
$\Gamma_{(\mathrm{had})}$ [GeV]	1.7444 ± 0.0020	2.4968 ± 0.0011
$\Gamma_{(\mathrm{inv})}$ [MeV]	499.0 ± 1.5	501.65 ± 0.11
$\Gamma_{(\ell^+\ell^-)}$ [MeV]	83.984 ± 0.086	83.996 ± 0.021
σ_{had} [nb]	41.541 ± 0.037	41.467 ± 0.009
R_e	20.804 ± 0.050	20.756 ± 0.011
R_μ	20.785 ± 0.033	20.756 ± 0.011
R_τ	20.764 ± 0.045	20.801 ± 0.011
R_b	0.21629 ± 0.00066	0.21578 ± 0.00010
R_c	0.1721 ± 0.0030	0.17230 ± 0.00004
$A_{FB}^{(0,e)}$	0.0145 ± 0.0025	0.01622 ± 0.00025
$A_{FB}^{(0,\mu)}$	0.0169 ± 0.0013	0.01622 ± 0.00025
$A_{FB}^{(0,\tau)}$	0.0188 ± 0.0017	0.01622 ± 0.00025
$A_{FB}^{(0,b)}$	0.0992 ± 0.0016	0.1031 ± 0.0008
$A_{FB}^{(0,c)}$	0.0707 ± 0.0035	0.0737 ± 0.0006
$A_{FB}^{(0,s)}$	0.0976 ± 0.0114	0.1032 ± 0.0008
$\bar{s}_\ell^2(A_{FB}^{(0,q)})$	0.2324 ± 0.0012	0.23152 ± 0.00014
A_e	0.15138 ± 0.00216	0.1471 ± 0.0011
A_μ	0.142 ± 0.015	0.1471 ± 0.0011
A_τ	0.136 ± 0.015	0.1471 ± 0.0011
A_b	0.923 ± 0.020	0.9347 ± 0.0001
A_c	0.670 ± 0.027	0.6678 ± 0.0005
A_s	0.895 ± 0.091	0.9356 ± 0.0001
g_L^2	0.30005 ± 0.00137	0.30378 ± 0.00021
g_R^2	0.03076 ± 0.00110	0.03006 ± 0.00003
g_V^2	-0.040 ± 0.015	-0.0396 ± 0.0003
g_A^2	-0.507 ± 0.014	-0.5064 ± 0.0001
A_{PV}	-1.31 ± 0.17	-1.53 ± 0.02
$Q_W(Cs)$	-72.62 ± 0.46	-73.17 ± 0.03
$Q_W(Tl)$	-116.6 ± 3.7	-116.78 ± 0.05
$\frac{\Gamma(b\to s\gamma)}{\Gamma(b\to Xe\nu)}$	$3.35^{+0.50}_{-0.44} \times 10^{-3}$	$(3.22 \pm 0.09) \times 10^{-3}$
$\frac{1}{2}(g_\mu - 2 - \frac{\alpha}{\pi})$	4511.07 ± 0.82	4509.82 ± 0.10
τ_τ [fs]	$290. \pm 0.58$	291.87 ± 1.76

Table 2.2: Observables calculated via the Standard Model and their experimental values [7]. Note that this is a global fit of the world's available data.

2.3.2 Flavor Hierarchy Problem

The masses of the fundamental particles vary widely. If the mass of the top quark was the same as an elephant, the mass of the electron would be approximately that of a small flea on the elephant. The ratio of top quark to electron masses is over 10^5. Why are the particle masses so varied?

This is known as the *Flavor Hierarchy Problem.*

2.3.3 Neutrino Mass

In the 1970s, experiments detecting the neutrinos created by the solar nuclear cycle measured only a fraction of the expected value [8]. This caused a major problem because otherwise the solar cycle fit very well with experiment. This deficiency became known as the *solar neutrino problem.*

One proposed solution to the solar neutrino problem was *neutrino oscillation.* The electron neutrinos from the sun arrived at the earth as electron, muon, and tau neutrinos. The neutrinos interact in flavor states – ν_e, μ_μ, and ν_τ – but they travel in mass states – ν_1, ν_2, and ν_3 – which are a linear combination of the flavor states:

$$\begin{pmatrix} \nu_1 \\ \nu_2 \\ \nu_3 \end{pmatrix} = \begin{pmatrix} U_{e1} & U_{\mu 1} & U_{\tau 1} \\ U_{e2} & U_{\mu 2} & U_{\tau 2} \\ U_{e3} & U_{\mu 3} & U_{\tau 3} \end{pmatrix} \begin{pmatrix} \nu_e \\ \nu_\mu \\ \nu_\tau \end{pmatrix} \tag{2.69}$$

where the U_{ij}'s are mixing parameters. Neutrino oscillations were compellingly observed at both Sudbury Neutrino Observatory (SNO) [9] and Super-Kamiokande (SK) [10]. In addition to solar neutrinos, SK also observed that the atmospheric neutrinos, produced by cosmic rays, have different upward- and downward-going flux. This is because the upward-going neutrinos have had more time to oscillate into a different type.

The sun does emit electron neutrinos; however, they travel to the earth in mass states. Upon arrival the neutrinos can interact in the detector. Due to oscillations, each mass neutrino has a certain probably of interacting as an electron neutrino or a muon neutrino or a tau neutrino. When an experiment is set up to measure electron neutrinos, it actually measures only a portion of the neutrinos arriving from the sun. The actual percent of each type of neutrino depends on the energy of the neutrinos, the distance traveled, and the mass difference between the neutrino mass states. Recently, SNO detected all types of neutrinos coming from the sun; this result agrees the solar theory, solving the solar neutrino problem.

Neutrino oscillation can only occur if there are mass differences between the neutrino mass states. Suddenly, neutrinos have a mass – a completely unexpected development. The Standard Model assumes massless neutrinos. This was a complete surprise to the high energy physics community.

However, the discovery of neutrino mass has raised still more questions. From the oscillations, it is possible to determine the difference between the masses squared, but not the actual value of the masses. In addition to the finding the neutrino masses m_{ν_i}, we are also interested in knowing the value mixing parameters U_{ij} and whether the neutrinos are Dirac or Majorana particles. A Dirac particle has a partner antiparticle, while a Majorana particle is its own antiparticle.

A new model needs to explain neutrino mass and mixing since the Standard Model assumes neutrinos are massless.

2.3.4 Missing Higgs Particle

The Higgs particle – essential to breaking the electroweak interaction and giving particles mass – has not been detected. Precision electroweak measurements give a preferred Higgs mass of less than 189 GeV. The optimal Higgs mass is 89^{+38}_{-28} GeV [7].

Electroweak precision data combined with the Large Electron-Positron (LEP) Collider direct search allows a Higgs mass as high as 189 GeV [7]. The Large Electron-Positron (LEP) Collider found a lower bound on the Higgs mass of 114 GeV [7]. The Tevatron will shortly reach this sensitivity, and may push up the bound or find the Higgs. The preferred values are presented in Fig. 2.1

[11]. The absence of the Higgs has lead to increased interest in more complex Higgs sector theories to explain why a light Higgs has not been detected.

Currently, the data neither confirms nor rules out the Standard Model, but the allowed region is narrowing. To agree with current data a Standard Model Higgs must have a mass $m_H > 114$ GeV. Electroweak precision data also limits

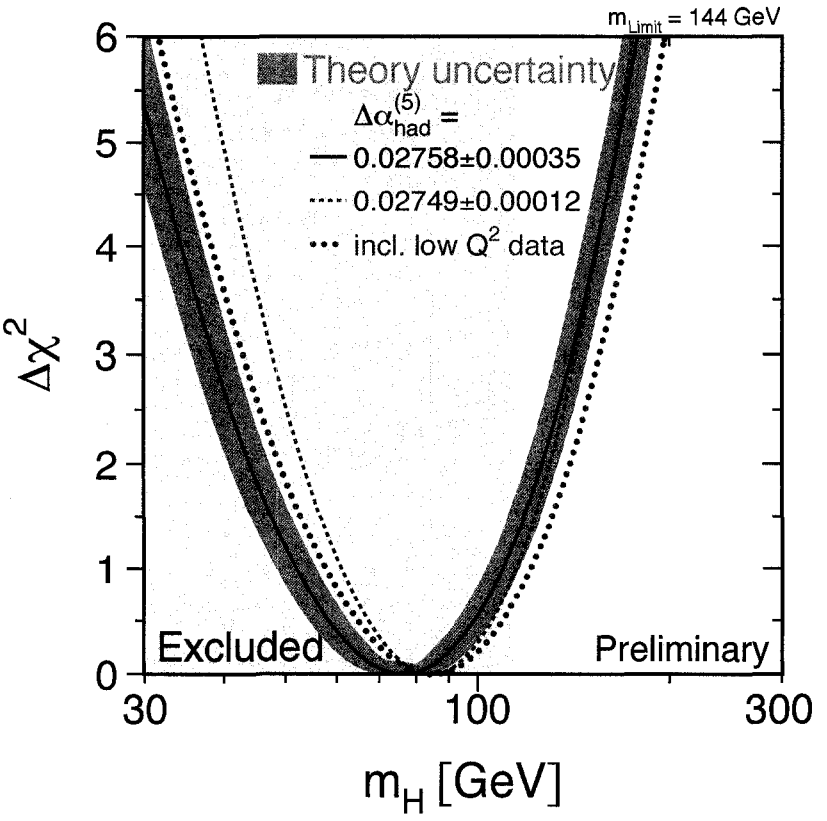

Figure 2.1: The theoretically allowed and the experimentally excluded mass region for the Higgs [11]. This plots the how well a given Higgs mass predicts the SM parameters. Varying the hadron vacuum polarization $\Delta\alpha^{(5)}_{\text{had}}$ does not significantly alter the results.

$m_H < 189$ GeV [7].

2.4 Solutions

Hundreds of solutions have been proposed to solve one or more problems with the Standard Model. Here, we will consider only two classes of solutions: extra dimensions and the addition of a fourth generation of matter.

2.4.1 Extra Dimensions

Extra dimensions can solve the gauge hierarchy problem. There are two explanations for why we not yet observed extra dimensions: first, the dimensions are smaller than we can measure, or, second, we cannot travel in the extra dimensions. Frequently, small dimensions are considered to be "rolled up" dimensions. If you keep traveling in the extra dimension you will eventually return to the point you began. This is known as the *compactification* of the dimension.

Consider single particles traveling in a compactified extra dimension, z. In our four dimensional world, we could not observe the travel in the extra dimension. We would, however, be able to measure the total energy of the particle and its momentum. From $E^2 = p^2 + m^2$, one can rewrite the energy as $E^2 = p_{4\mathrm{D}}^2 + (p_z^2 + m^2)$, where p_z is the momentum of the particle in the

extra dimensions. Since we can only measure the momentum in our own four-dimensional world, the momentum will appear as part of an effective mass, M_{eff}, the energy squared is

$$E^2 = p_{4\text{D}}^2 + M_{\text{eff}}^2. \tag{2.70}$$

Since the extra dimension is closed, the momenta allowed are discrete or quantized. Assuming the extra dimension is compactified onto a circle of radius R, the allowed momenta are $p_z^2 = \frac{n^2}{R^2}$. These heavy particles are known as Kaluza-Klein particles. The resulting spectrum is a tower of Kaluza-Klein (KK) particles – each heavier than the previous:

$$M_{\text{eff}}^2 = m^2 + \frac{n^2}{R^2}. \tag{2.71}$$

These heavier particles can also be described as Fourier modes of the original, four dimensional particle.

Current experimental data forces the inverse radius of a single compactified universal extra dimension to be $> 300 - 500$ GeV [7].

Warped Extra Dimensions

The mere existence of an extra dimension does not solve the problems of the Standard Model. There are some types of extra dimensional models that do solve some of these problems. In particular, the Randall-Sundrum (RS) model, or warped extra dimensions, can solve both the gauge and flavor hierarchy problems.

The metric of the Randall-Sundrum model [12] is

$$ds^2 = e^{-2\sigma(z)}\eta_{\mu\nu}dx^\mu dx^\nu + dz^2 \tag{2.72}$$

where $\sigma(z) = k|z|$, k is related to the curvature of the Anti-de Sitter, AdS_5, space, $\eta_{\mu\nu}$ is the flat-space metric, and z is the fifth coordinate. The fifth dimension is compactified to a S^1/Z_2 space with radius R bounded by four dimensional branes at the fixed points $z = 0$ and $z = \pi R$. These four dimensional branes are called the Planck brane ($z = 0$) and the TeV brane ($z = \pi R$).

We will now present the masses and couplings of gauge bosons and fermions, when they propagate in the bulk. More detailed derivations of these results can be found in [13, 14, 15, 16, 17, 18, 19].

The equation of motion for a bulk gauge field is given by [13, 14, 15, 16, 17]

$$\frac{1}{\sqrt{-G}}\partial_M(\sqrt{-G}\ G^{MN}G^{RS}F_{NS}) - M_A^2 G^{RS}A_S = 0 \tag{2.73}$$

where M_A arises from spontaneous symmetry breaking, G^{MN} is the above metric, Eq. (2.72), and $\sqrt{-G} = e^{-4\sigma}$. This can be rewritten as

$$[e^{2\sigma}\eta_{\rho\nu}\partial^\rho\partial^\nu + e^{2\sigma}\partial_5(e^{-2\sigma}\partial_5) - M_A^2]A(x_\mu, z) = 0 \tag{2.74}$$

The Higgs field is localized on the TeV brane, and thus $M_A^2 = \frac{1}{2}g_5^2 v^2 \delta(z - \pi R)$. The vacuum expectation value is of the order of the Planck mass.

Decomposing the gauge field (using the gauge $A_5 = \partial_\mu A^\mu = 0$), one has

$$A(x_\mu, z) = \frac{1}{\sqrt{2\pi R}} \sum_{n=0}^{\infty} A^{(n)}(x_\mu) f_n^A(z) \tag{2.75}$$

where the orthogonality condition is

$$\frac{1}{2\pi R} \int_{-\pi R}^{\pi R} dy f_n^A(z) f_m^A(z) = \delta_{mn} \tag{2.76}$$

Plugging the decomposition into the equation of motion, one can solve the equation and find [13, 14, 17]

$$f_n^A(z) = \frac{e^\sigma}{N}\left[J_1\left(\frac{m_n}{k}e^\sigma\right) + b_1(m_n)Y_1\left(\frac{m_n}{k}\right)\right] \tag{2.77}$$

The values of m_n and b are given by the boundary conditions, and N by the normalization condition. Note that the mass term does not enter into

this equation; it will only affect the boundary conditions at the TeV brane. Imposing these conditions gives the zero-mode mass [17]

$$m_0^2 = g_5^2 v^2 e^{-2\pi kR} \left(1 + \mathcal{O}(g_5^2 v^2 e^{-2\pi kR}/M_1^2)\right) \tag{2.78}$$

where the mass of the first excited KK state $M_1 \sim \mathcal{O}(1/R) \sim 10^{-32}$. Note that a gauge hierarchy naturally appears. The higher order correction causes a tree-level shift in the W and Z masses, affecting electroweak precision data if the KK scale is too small, leading to many of the bounds noted in the previous section. The masses of the KK excitations of the gauge bosons are related to zeroes of the Bessel functions. One can add brane kinetic terms for the gauge bosons; this will be discussed in Chapter 4.

A straightforward way of seeing how the RS model solves the gauge hierarchy problem is as follows. The action involving the scalar field is

$$\int d^4x\, dz \sqrt{-g} \left(g^{\mu\nu} D_\mu \phi D_\nu \phi - \lambda(\phi^2 - v^2)^2\right) \delta(z - \pi R) \tag{2.79}$$

where $g = \det(g_{\mu\nu})$. Since $\sqrt{-g} = e^{-4\sigma}$, one can normalize the kinetic term by $\phi \to e^{\sigma}\phi$. This has the effect of $v \to v\, e^{-\pi kR}$ which solves the gauge hierarchy problem, for $kR \sim 11$.

If the fermions are on the TeV brane, then, as shown in [13, 14], their

couplings to the gauge bosons are of the form

$$\mathcal{L} = -g\overline{\psi}\gamma^{\mu}\left(A_{\mu}^{(0)} + \sqrt{2\pi kR}\sum_{n=1}^{\infty} A_{\mu}^{(n)}\right)\psi \tag{2.80}$$

which gives an enhancement of $\sqrt{2\pi kR} \simeq 8.4$ in the coupling. This changes substantially if the fermions are in the bulk.

When fermions are in the bulk [17, 18, 19], they can have two possible transformation properties under the orbifold Z_2 symmetry: $\psi = \pm\gamma_5\psi$. As a result, $\overline{\psi}\psi$ is odd under the Z_2, and thus the Dirac mass term must originate from coupling to a Z_2 odd scalar field. This mass term can then be written as $m_{\psi} = c\frac{d\sigma}{dz}$, where $\sigma = k|z|$. As we will see shortly, the parameter c will be crucial in determining the properties of the fermions.

As before, one can expand the fields and determine the wavefunctions and masses of the fermions. One expands

$$\psi(x^{\mu}, z) = \frac{1}{2\pi R}\sum_{n=0}^{\infty}\psi^{n}(x^{\mu})e^{2\sigma}f_n(z) \tag{2.81}$$

where the normalization condition is

$$\frac{1}{2\pi R}\int_{-\pi R}^{\pi R} dz\; e^{\sigma}f_m(z)f_n(z) = \delta_{mn} \tag{2.82}$$

and the factor of $e^{2\sigma}$ comes from the spin connection.

Plugging into the Dirac equation, one finds the zero mode wave function is simply (we suppress flavor indices and neglect flavor mixing)

$$f_0(z) = \frac{e^{-c\sigma}}{N_0} \tag{2.83}$$

and the KK fermion wave functions are

$$f_n(z) = \frac{e^{\sigma/2}}{N_n}\left[J_\alpha\left(\frac{m_n}{k}e^{\sigma}\right) + b_\alpha(m_n)Y_\alpha\left(\frac{m_n}{k}\right)\right] \tag{2.84}$$

where $\alpha = |c \pm \frac{1}{2}|$ for $\psi_{L,R}$. The masses and b_α are given by the boundary conditions.

The zero-mode wave function is sufficiently simple that the normalization constant N_o can be determined easily to be

$$N_o^2 = \frac{e^{2\pi kR(1/2-c)} - 1}{2\pi kR(1/2-c)} \tag{2.85}$$

From this, one can see that if $c > 1/2$, the zero mode fermions will be localized near the Planck ($z = 0$) brane, while for $c < 1/2$, they will be localized near the TeV ($z = \pi R$) brane.

The zero modes acquire mass through coupling to the Higgs field on the

TeV brane (here, we include flavor indices)

$$m_{ij} = \int_{-\pi R}^{\pi R} \frac{dz}{2\pi R} \lambda_{ij}^5 \langle H(z) \rangle f_{0iL}(z) f_{0jR}(z) \tag{2.86}$$

and using $\langle H(z) \rangle = v\delta(z - \pi R)/k$, one finds

$$m_{ij} = \frac{\lambda_{ij}^4 v}{\pi k R} f_{0iL}(\pi R) f_{0jR}(\pi R) \tag{2.87}$$

where the dimensionless 4-D coupling $\lambda_{ij}^4 = \lambda_{ij}^5 \sqrt{k}$.

This demonstrates how a huge fermion mass hierarchy can arise. For $c < 1/2$, the wave function $f_0(\pi R)$ varies as $\sqrt{1-2c}$, but for $c > 1/2$ varies as $e^{-c\pi kR}$. Since $\pi kR \simeq 35$, this exponential suppression can lead to a hierarchy. Huber [17] shows explicitly how mild variations in c can lead to the observed mass spectrum, and can also lead to reasonable flavor mixing.

The couplings between gauge bosons and fermions come from the 5-D term

$$\int d^4x dz \sqrt{-G} g_5 \overline{\psi}(x,z) i\gamma^\mu A_\mu(x,z) \psi(x,z) \tag{2.88}$$

which induces 4D-couplings

$$g_{ijn} = \frac{g_5}{(2\pi R)^{3/2}} \int_{-\pi R}^{\pi R} e^\sigma f_i(z) f_j(z) f_n^A(z) dz. \tag{2.89}$$

From this, we can determine all gauge-boson couplings to fermions.

Note that for a zero-mode massless gauge boson, $f_0^A = 1$, and the result just gives the normalization condition, giving $g_{ij0} = \delta_{ij} g_5/\sqrt{2\pi R}$, thus fermion couplings to the zero-mode are KK level conserving.

For our calculation, we will need the coupling of a KK gauge boson to zero-mode (or Standard Model) fermions, which is then[2]

$$g^{(n)} = g\left(\frac{1-2c}{e^{(1-2c)\pi kR}-1}\right)\frac{k}{N_0} \cdot \int_0^{\pi R} dz\, e^{\sigma} e^{(1-2c)\sigma}\left[J_1\left(\frac{m_n}{k}e^{\sigma}\right) + b_1(m_n) Y_1\left(\frac{m_n}{k}\right)\right]. \tag{2.90}$$

These are plotted in [18] for $n = 1, 2, 3$ as a function of c. This coupling actually depends on the zero-mode fermions' location in the bulk. For c large and negative (so the fermion is very close to the TeV brane), the coupling ratio reaches $\sqrt{2\pi kR} \simeq 8.4$, as discussed earlier. As c increases, they become smaller, vanishing in the conformal limit $c = 1/2$, and then reach a constant value of approximately -0.2 for $c > 1/2$.

This scenario is very attractive, due to the manner in which the fermion mass hierarchy naturally arises. We can see that fermions near the TeV brane couple more strongly than those away from the TeV brane. Since the top quark is closest to the TeV brane, one expects the biggest effects to arise in top-quark

[2]In [18], the first factor of e^{σ} in the integral is missing – this is entirely typographical and does not affect their results.

processes, and if the KK scale is much larger than 10 TeV, these processes may be the first signature.

We will turn to top pair production in warped extra dimensions in Chapter 4. Several variations of warped extra dimensions will be explored.

2.4.2 Fourth Generation of Matter

Having discovered three families of particles, it is natural to wonder whether they are only families or if still heavier families of matter exist. The Z boson decays into a neutrino-antineutrino pair. The Z width can be fit to the various numbers of families, see Fig. 2.2 [20].

However this fit assumed that all neutrinos were massless. With the recent discovery of neutrino mass, there is currently nothing to limit possible neutrino mass. The Z cannot decay into any of these new neutrinos; this means that the mass of the new neutrino must be greater than half of the Z mass:

$$m_N > \frac{1}{2} m_Z = 46\,\text{GeV}. \tag{2.91}$$

It is no longer absurd to consider the existence of heavy neutrinos. Current searches for heavy neutrinos have excluded heavy neutrinos that decay into the three light neutrinos to greater than $\sim 80 - 100$ GeV [7]. However if the heavy neutrino is stable and does not decay into lighter neutrinos, then the mass is

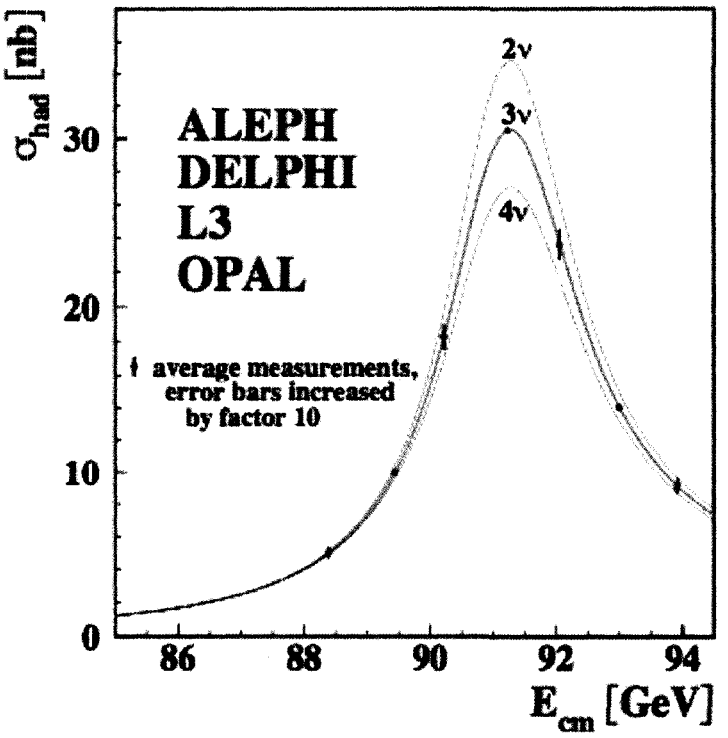

Figure 2.2: Fitting various numbers of neutrinos to the width of the Z boson [20].

limited only by the width of the Z ($m_N > 46$ GeV).

A sequential generation is a fourth generation that interacts just like the three standard generations. There is a $+2/3$ quark U and a $-1/3$ quark D in addition to a heavy Dirac neutrino N and heavy charged lepton L, see Table 2.3. There is a doublet of left-handed quarks, $(U, D)_L$, and right-handed quark singlets, $(U)_R$ and $(D)_R$.

Interest in a fourth generation has waxed and waned over the years. After precision measurements of the Z width showed that there are precisely three

Particle	Flavor				$Q/\|e\|$
leptons	e	μ	τ	L	-1
	ν_e	ν_μ	ν_τ	N	0
quarks	u	c	t	U	$+\frac{2}{3}$
	d	s	b	D	$-\frac{1}{3}$

Table 2.3: Particles in a sequential four generation model.

weakly interacting neutrinos [7], it became clear that the neutrino mass of a fourth generation would have to exceed 45 GeV and interest faded.

During the 1990s there was intensive study of the phenomenology of additional quarks and leptons which were *not* sequential [21, 22, 23, 24, 25]. Many grand unified theories have additional fermions, such as vectorlike isosinglet quarks and leptons, additional vectorlike states arise in gauge-mediated supersymmetry breaking models, and many additional models contain mirrorlike fermions. These models are still of interest, but they do not require sequential fermions (although they can accommodate them).

Interest in a sequential fourth generation faded further with studies of precision electroweak constraints. The recent Particle Data Group analysis claimed that "An extra generation of ordinary fermions is excluded at the 99.999% CL" [7]. However, this analysis assumes a mass-degenerate fourth generation. Since one of the most striking features of the mass spectrum of the first three generations is the wide range of masses, such an assumption may not be justifiable.

Analyses of the effects of a non-degenerate sequential fourth generation

originally focused on the case where the neutrino mass was of $O(50)$ GeV [26, 27, 28, 29] and used 2001 electroweak data. A comprehensive analysis of the current status of precision electroweak fits and a fourth generation was recently carried out by Kribs, Plehn, Spannowsky and Tait [30]. They noted that the constraints on the parameters from combined electroweak data have been determined by both the LEP Electroweak Working Group [31] and the Particle Data Group [7]. Since the two groups used somewhat different datasets, their results differ by roughly one standard deviation from each other (see [30] for a detailed discussion of the differences). Kribs *et al.* used the LEP Electroweak Working Group results, and found that a substantial region of fourth-generation parameter space is in agreement with all experimental constraints. In this region of parameter space, the mass splitting between the U and D quarks is between 50 and 80 GeV. Bounds on the mass splitting between the charged lepton, L, and the neutrino, N, are less constrained since one considers both Dirac and Majorana neutrino masses [32, 33, 34].

Thus, we thus see that precision electroweak data do not exclude a sequential fourth generation. U and D quark production at the Large Hadron Collider (LHC) will be relatively easy to detect. However, the heavy charged lepton, L, will be substantially more difficult to detect, primarily due to large backgrounds. Early LHC and Superconducting Super Collider, SSC, studies [35, 36]

made the assumption of a massless fourth generation neutrino, and still concluded that detecting a heavy lepton with a mass greater than 250 GeV might not be possible. Calculations of heavy lepton production exist [37] but do not include any discussion of signatures or backgrounds. Therefore, it is likely that a heavy charged lepton with a mass greater than 250 GeV will not be detected at the LHC.

2.5 Experiment Summary

There have been many experiments in particle physics since the first collider in the 1930s. We will discuss recent and upcoming collider experiments.

2.5.1 Large Electron-Positron Collider

The Large Electron-Posistron (LEP) Collider ran from 1989 to 2000 at CERN in Geneva, Switzerland. It reached a maximum beam energy of a little over 100 GeV. The luminosity varied from $24 \times 10^{30}\text{cm}^{-2}\text{s}^{-1}$ at the Z^0 peak to $100 \times 10^{30}\text{cm}^{-2}\text{s}^{-1}$ at energies above 90 GeV. Electrons and positrons collided every 20 μs [7].

The four detectors at LEP – ALEPH (Apparatus for LEP Physics), DELPHI (Detector with Lepton Photon and Hadron Identification), OPAL (an Omni Purpose Apparatus for LEP), and L3 (named for its location on the

accelerator ring) – successfully explored properties of the W and Z bosons, including precise measurements of the masses and width of the Z.

2.5.2 Tevatron

The Tevatron is a proton-antiproton collider that has been running since 1987 at Fermilab in Batavia, Illinois, United States. It has a maximum center-of-mass energy for 0.98 TeV and luminosity of 3.2×10^{32} cm^{-2}s^{-1}. Collisions occur every 396 ns [7].

The Tevatron is both a great success and a disappointment. The detectors at the Tevatron – CDF (Collider Detector at Fermilab) and DØ (DZero for its location on the accelerator ring) – discovered the top quark in 1995. However, it has not yet found the Higgs. The Tevatron is expected to run until the Large Hadron Collider has collected a larger dataset than the Tevatron.

2.5.3 Large Hadron Collider

Built in the LEP tunnel at CERN in Geneva, Switzerland, the Large Hadron Collider (LHC) is currently in the final stages of installation and commissioning. The first proton beams should be injected in summer 2008. This is the first experiment in decades where the particle physics community has no idea what to expect. The LHC will collide two proton beams every 25 ns at a maximum

beam energy of 7 TeV and a luminosity of 1.0×10^{34} $cm^{-2}s^{-1}$.

The higher energy and the increased number of particles will create many more events in each collision. This leads to huge backgrounds that will take some time to understand. This could make it difficult to detect new physics. There are two major detectors at the LHC – ATLAS (A Toroidal LHC ApparatuS) and CMS (Compact Muon Solenoid). Their different designs and and analysis will help ensure accuracy at the LHC.

2.5.4 International Linear Collider

The International Linear Collider (ILC) is a proposed electron-positron collider. It is expected to have a center of mass energy of 0.5 TeV with a later upgrade to 1 TeV. Although it has lower energy that the LHC, electron-positron annihilation can be much more precisely calculated than the proton-antiproton annihilation in the LHC. Further since the electron and positron completely annihilate each other, all of the center-of-mass energy is available for the interaction. At hadron colliders (such as the LHC) only a some of the energy is available, the rest remains with the leftover initial particles. Since the ILC will not have any leftover initial particles remaining and it is a basic annihilation interaction, the backgrounds are much better understood allowing more precise measurements to be conducted.

Still in the design phase, the site for the ILC has not been chosen. The combination of the LHC and the ILC will allow maximum discovery potential and precise measurements. The classic combination of hadron and lepton colliders is the discovery of the Z boson at the Super Proton Synchrotron in 1983 and followed precise measurements at LEP.

2.6 Conclusions

The Standard Model has successfully predicted experimental results for the last forty years. However some problems exists. This opens the door for new physics beyond the SM – particularly the existence of extra dimensions and a fourth generation of matter. We will now examine three proposed methods to detect new physics.

Chapter 3

Kaluza-Klein Mesons at the International Linear Collider

In order for hadronic bound states to form, the constituents must have lifetimes longer than the hadronization time scale, of $\mathcal{O}(10^{-24})$ seconds. When the top quark was discovered to have a mass much larger than 130 GeV, it was clear that hadrons containing top quarks could not exist. In models beyond the Standard Model, strongly interacting states with sufficiently long lifetimes can certainly exist. For example, a fourth generation quark, with very small mixings with the lighter generations, could exist, and its bound states have been studied [38, 39, 40]. Also in supersymmetric models where the gravitino is the lightest supersymmetric partner and a squark is the next-to-lightest, squarkonium [41,

42, 43] and mesino [44] bound states have been studied.

Recently Carone *et al.* [45] considered bound states in models with universal extra dimensions [46]. In these models, all particles propagate in the extra dimensions and the Kaluza-Klein (KK) parity makes the lightest KK particle (LKP) stable. It also allows compactification of the extra dimensions to be very low, as low as 300 GeV. Since the other KK states have masses only slightly greater than this lightest state, they are incredibly long-lived. Carone *et al.* analyzed the bound states of a KK quark and its KK antiquark, also called KK quarkonia. In particular, the isosinglet KK quarks will decay into a monochromatic quark and missing energy, leading to dramatic resonances, similar to the J/ψ and Υ states, with very clear signatures. This Chapter studies the possibility of detecting KK mesons, consisting of a KK quark and a zero-mode (or Standard Model) antiquark (or vice versa).

3.1 Universal Extra Dimensions (UED)

In universal extra dimensions at tree level, the masses of the lightest excitations of the quarks, q^1, are degenerate with most of the other KK states. Radiative corrections [47] will break this degeneracy, with the KK quarks being roughly $50 - 100$ GeV heavier than the LKP. Cheng, Matchev and Schmaltz [47] calculated the widths for the KK quarks and found the isosinglet d^1, s^1, and b^1

widths were $O(5-10)$ MeV, for the decay into a quark and LKP (consisting mostly of the KK photon) to exist. The widths of the $Q = 2/3$ isosinglet KK quarks are 4 times larger than those of the $Q = -1/3$ KK quarks and will not be discussed further.

3.2 Production Processes

In their paper, Carone *et al.* claimed that the isosinglet KK top quark was very long-lived (with a width of tens of keV), but neglected the mixing between the isosinglet and isodoublet KK quarks [45]. The mass matrix for the KK top modes is [47]

$$\begin{pmatrix} 1/R + \delta m_{T^1} & m_{\text{top}} \\ m_{\text{top}} & -1/R - \delta m_{t^1} \end{pmatrix} \tag{3.1}$$

where the δm's are small radiative corrections. This leads to a mixing angle which is given by

$$\tan 2\theta_1 = \frac{2m_{\text{top}}R}{2 + \delta m_{T^1}R + \delta m_{t^1}R}. \tag{3.2}$$

This factor leads to an isosinglet top quark coupling to the b quark and the KK W boson given by the usual coupling times $\sin\theta_1$). This allows the KK top to decay directly into a b quark and KK W boson. We find the lifetime

(assuming $|V_{tb}| = 1$ to be given by

$$\Gamma = \sin^2\theta_1 \frac{G_F}{\sqrt{2}} \frac{M_W^2}{3\pi m_{t^1}^3 M_{W^1}^2} \left(m_{t^1}^2 - M_{W^1}^2\right)\left(m_{t^1}^2 + 2M_{W^1}^2\right) \tag{3.3}$$

For $1/R \sim 500$ GeV, Γ is 10 MeV. The signature for this decay will be a monochromatic b quark, a monochromatic lepton, and missing energy [45].

Given this width, hadronization will occur. How could one detect the resulting KK mesons? Recall how B mesons are detected. There are three signatures. First, the $\Upsilon(4s)$ resonance is just above the threshold for a pair of B mesons, thus the strong decay causes the $\Upsilon(4s)$ to significantly broader than the lighter three Υ states. Second, well above threshold, one can look at the B meson decay. And third, one can look for $B - \bar{B}$ mixing and like sign dileptons.

3.2.1 Decay of KK quarkonia on resonance

One can produce copious numbers of $\bar{q}^1 q^1$ mesons at a linear collider on resonance. Above the threshold energy the widths of these resonances become much larger. In the WKB approximation, the number of heavy meson states below the quarkonium threshold, N_T, is approximately [48]

$$N_T(Q\bar{Q}) \simeq 2\sqrt{m_Q/m_c} \tag{3.4}$$

which gives 2 for the J/ψ system, 3 for the Υ system, and approximately 12 for the KK quarkonium system. Thus one must look at the $13s$ state of KK quarkonium to see pair production of KK mesons. However the production cross-sections scales $1/n^3$ [45], allowing only the first 3 resonances to be detected clearly. Hence, it is not possible to detect KK mesons via pair production on the KK quarkonium resonance.

3.2.2 Decay of mesons well above threshold

Is it possible to detect the KK mesons through their decays well above threshold? Recall that the KK quark will decay into a large amount of missing energy (typically 80-90% of the particle's mass) and a soft, monochromatic quark [49, 50]. Given the expected beamstrahlung of several GeV [49, 50] and beam resolution of at least 50 MeV in addition to the huge amount of missing energy, it is difficult to see a possible way to distinguish between a free KK quark and one decaying in a meson.

One can look at the KK meson decay, rather than the spectator quark decay. Ignoring Cabibbo-Kobayashi-Maskawa (CKM) mixing angles, the KK meson can annihilate through a KK W boson into a KK electron and a neutrino. The KK electron then decays into a KK photon and an electron. The width is given

by

$$\frac{f_M^2 g^4}{64\pi m_{q^1}^3} \frac{m_{e^1}^2 \left(m_{q^1}^2 - m_{e^1}^2\right)^2}{\left(m_{q^1}^2 - m_{W^1}^2\right)^2} \tag{3.5}$$

where f_M is the meson decay constant, which is of the order of the QCD scale Λ_{QCD}. Numerically, this is $O\left(10^{-7}\right)$ GeV, which is negligible compared with the free KK quark width of a few MeV.

One can also consider the "electromagnetic" decay of a flavor neutral KK meson into a KK photon and a zero-mode photon (analogous to $\pi \leftarrow \gamma\gamma$). We have calculated this width and find it to be approximately 1×10^{-10} GeV, which is also negligible. This is not surprising, since the decay constants give factors of Λ_{QCD}^2, which is significantly smaller than then other scales in the problem.

3.2.3 KK meson mixing

In the case of the isosinglet KK top quark, the mixing angles in the decay to a KK W and a b quark, the sign of the lepton in the decay of the KK W tags its charge and thus the charge of the KK top quark. With mixing, one would see two like sign monochromatic leptons - a striking signature. Sarid and Thomas [44] showed that a mesino-antimesino oscillation, through this signature, could allow the discovery of mesinos, even if they could not otherwise be detected. One must calculate the box diagram in which a W and a KK W are exchanged. For the KK meson $t^1 q$, we find the mass difference, Δm, between the KK meson

and its antiparticle to be

$$\Delta m = 2\left(\frac{G_F\alpha}{\sqrt{2}8\pi}\right)\left(\frac{1}{M_W\sin\theta_W}\right)^2 \sum_{Q,Q^1}\Re\left[M_W^4 V_{qQ}^* V_{t^1Q} V_{Q^1q}^* V_{Q^1t^1}\frac{4}{3}f_{t^1}^2 m_{t^1q} A\left(m_Q, m_{Q^1}\right)\right] \quad (3.6)$$

where Q is summed over d, s, b and Q^1 is summed over d^1, s^1, b^1 and

$$A\left(m_Q, m_{Q^1}\right) = -\sum_{i=1}^{4}\frac{M_i^4 \ln M_i^2}{\Pi_{j\neq i}\left(M_i^2 - M_j^2\right)} \quad (3.7)$$

where $M_i = (M_Q, M_W, M_{Q^1}, M_{W^1})$. Alas, the mass difference is completely negligible, of the order of a few eV. The reason for this is a double-Glashow-Illiopoulos-Maiani (GIM) mechanism - the d, s, and b quarks are nearly degenerate (they are all very light compared to the other scales in the problem) and the d^1, s^1, and b^1 KK quarks are also, in universal extra dimensions, nearly degenerate as well. In the limit of exact degeneracy, the sum over the three generations will yield the product of two columns in the CKM elements from the first two CKM factors of Eq. (3.5) and the product of two rows from the latter two CKM elements. Alas, this mechanism will also fail to detect KK mesons.

This inability to detect KK mesons is in sharp contrast with bound states of fourth generation quarks and supersymmetric quarks. Fourth generation

quarks can have longer lifetime, neutral current decays (thus no missing energy) and the $Q = 2/3$ quark will give a large GIM violation. leading to large mixing. Supersymmetric quarks can also have longer lifetimes, less missing energy in their decays, and the mixing can occur through flavor-changing gluino interactions. While bound states in fourth generation quark and supersymmetry models are detectable, it appears that the Kaluza-Klein mesons are not.

Chapter 4

Top Quark Production in Randall-Sundrum Models at the International Linear Collider

For the past quarter of a century, two of the most promising solutions to the gauge hierarchy problem have been supersymmetry and technicolor. These extensions of the Standard Model have provided some of the primary motivations for the LHC and the ILC, and have provided a rich framework for studying beyond the Standard Model phenomenology.

An alternative approach was provided several years ago by the Randall-Sundrum (RS1) model [12].

4.1 Randall-Sundrum Model

As discussed in Chapter 2, in the Randall-Sundrum (RS) model, spacetime is five-dimensional, with one dimension compactified on an S_1/Z_2 orbifold. The five-dimensional bulk geometry is a slice of anti-de Sitter (AdS_5) space. At the fixed points of the orbifold (at $z = 0, \pi R$), the slice is bounded by 3-branes of equal and opposite tension. The brane at $z = 0$ is referred to as the Planck brane, while the brane at $z = \pi R$ is referred to as the TeV brane. The curvature scale, k, and the length of the AdS_5 slice, πR, are expected to be of the order of the Planck mass, M_P and its inverse, respectively. The geometry then induces a effective scale on the TeV brane of the order of $M_P e^{-\pi kR}$. For $kR \simeq 11$, which is not particularly "fine-tuned", this scale is of the order of a TeV. If the Higgs field(s) live on the TeV brane, then the electroweak scale is naturally generated. Thus, the hierarchy problem is solved. There are several very nice reviews of the model that also discuss many of the issues discussed in the rest of this section [51, 52].

In the original model, only gravity propagated in the bulk and the Standard Model fields were confined to the TeV brane. Nonetheless, this leads to interesting collider effects from Kaluza-Klein (KK) graviton exchange [53]. It was realized at an early stage that a much richer phenomenology would arise if one allowed some of the Standard Model fields to propagate in the bulk.

Initially, the effects of gauge bosons in the bulk (with the Higgs field and fermions still confined to the TeV brane) were considered [13, 14]. In this model, the couplings of the fermions to the KK excitations of the gauge bosons are enhanced relative to the couplings to the zero-mode gauge bosons by a factor of $\sqrt{2\pi kR} \simeq 8.4$. These large couplings cause serious constraints [15, 54, 55] from precision electroweak measurements, with lower bounds ranging from $10 - 25$ TeV on the mass of the lowest lying KK excitation of the gauge bosons. Such a high mass would be beyond the reach of the LHC, and would also reintroduce the hierarchy problem (although at a much smaller level of fine-tuning).

One method of relaxing these constraints, with fermions still on the TeV brane, is to include brane-localized kinetic terms for the gauge fields. These terms should be present in general [56]. Their effects on couplings and masses were shown to be substantial in flat space [57], and an analysis [58] in the RS model showed that the lower bound on the lightest KK excitation mass could be substantially smaller.

An alternative approach to relaxing the constraints is to allow fermions to propagate in the bulk. This also gives the exciting possibility of explaining the large fermion mass hierarchies. With fermions in the bulk, the bounds from electroweak precision data were somewhat ameliorated [15, 18, 59, 60, 16, 61, 62]. In addition, since fermions are in the bulk, the couplings of the fermions

to the Higgs boson (which remains on the TeV brane) can be substantially suppressed by the geometric warp factor [18, 19, 63, 17]. For fermions near the TeV brane, the suppression is small, but for fermions far from the TeV brane, the suppression can be exponential, leading to large fermion mass hierarchies. The observed fermion mass hierarchy then becomes a matter of fermion geography. Huber [17] has shown explicitly how simple parameters of $O(1)$ can lead to the observed fermion mass hierarchy and mixings.

As shown by Agashe *et al.* [64], the model still had large contributions to the T parameter (which is "proportional to the difference between the W and Z self-energies at $Q^2 = 0$ [7]) in electroweak radiative corrections, forcing the KK scale to still be out of reach of the LHC. It also had large contributions to $Z \rightarrow \bar{b}b$. The reason is that the large top quark mass forces the top quark to be near the TeV brane, so that it can interact strongly with the Higgs. But since the left-handed top is paired with the left-handed bottom, the left-handed bottom will have to be near the TeV brane, and that leads to larger corrections to the $Z \rightarrow \bar{b}b$ rate. They showed that imposing a custodial isospin symmetry in the bulk (by enlarging the gauge group to $SU(2)_L \times SU(2)_R \times U(1)_{B-L}$) solves both of these problems, and allows the lowest lying KK states to have masses as low as a few TeV, within range of the LHC. These models are attractive in that the custodial isospin gauge symmetry of the bulk can be dual, through

the AdS/CFT correspondence, to a global isospin symmetry of the CFT [64].

There are other alternatives. Hewett, Petriello and Rizzo [65] consider putting the first two families in the bulk and the third on the brane, and alleviate these problems. This paper was the first to consider top pair production in Randall-Sundrum models at a linear collider, although it was in the context of the model with the third generation on the brane and used a common mass parameter for the other fermions. More recently, Carena *et al.* [62] show that brane kinetic terms for the fermions can also give good fits for relatively light KK masses. There are several introductions to brane kinetic terms [66, 67, 68] and many of these issues, including flavor changing neutral currents, were summarized by Moreau and Silva-Marcos [69], where they pointed out that the KK mass scale could be lowered to the few TeV mass scale without problems with precision electroweak data.

Our approach in this Chapter is somewhat different. We will not attempt to find ways to lower the KK masses to the range of the LHC, but will consider the possibility that these masses are in the $10 - 100$ TeV range. In this case, they will be out of reach of the LHC and ILC, and (except possibly in the lower end of the range for some models) will be insensitive to electroweak precision measurements (and any sensitivity can be eliminated with one of the techniques discussed above). Of course, there will be a hierarchy problem;

although substantially less of a problem than in standard grand unified theories, and we will not address that issue. In this scenario, what would the first experimental evidence be? Since the top quark is close to the TeV brane, effects of KK states on top pair production would be the most pronounced, and thus could be the first signature (more likely at the ILC, where higher precision measurements can be made). In this work, we study top pair production in a variety of RS models, and determine the reach of KK masses expected at the ILC.

In Chapter 2, the RS models were presented. In Section 4.2, we consider only the effects of KK gauge bosons, ignoring KK fermions. In Section 4.3, the effects of KK fermions and of brane kinetic terms are considered. Finally Section 4.4 contains our conclusions.

4.2 Effects of KK Gauge Bosons

4.2.1 Fermions on the brane

As discussed in the previous section, if all of the Standard Model fermions are on the brane, then their couplings to the KK gauge bosons are enhanced by a factor of $\sqrt{2\pi kR} \sim 8.4$. This will lead to substantial corrections to fermion pair production through the diagrams of Fig. 4.1. In this diagram, we neglect the

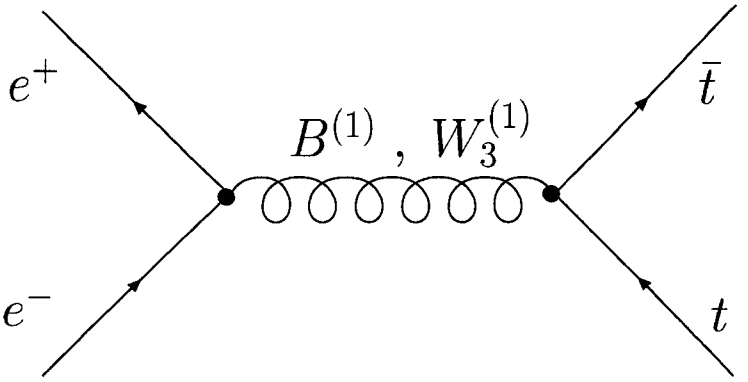

Figure 4.1: Tree-level diagrams affecting top pair production. The exchanged gauge bosons are the KK W_3 and KK B.

$n = 1$ weak mixing angle, which is defined as the rotation angle between the hypercharge and $SU(2)$ gauge bosons and their mass eigenstates. The reason for this is that mixing is due to electroweak symmetry breaking, and the scale of the KK gauge boson masses is much, much larger. This is similar to the case of universal extra dimensions [70] in which the weak mixing angle for the $n = 1$ states was shown to be $O(0.01)$.

The corrections to the top pair production cross-section can be easily calculated for the exchange of the $n = 1$ KK gauge bosons. Our results are given in Fig. 4.2 for $\sqrt{s} = 0.5, 1.0, 1.5$ TeV. The expected sensitivity of the ILC is approximately one percent, and thus the ILC will be able to probe masses up to 120 TeV (for $\sqrt{s} = 1.0$ TeV). Note that the interference is destructive. The sensitivity to high mass scales should not be surprising, since one expects the change in the cross-section to be approximately $2 \times (8.4)^2 \times \frac{s}{M_{KK}^2}$, and a one

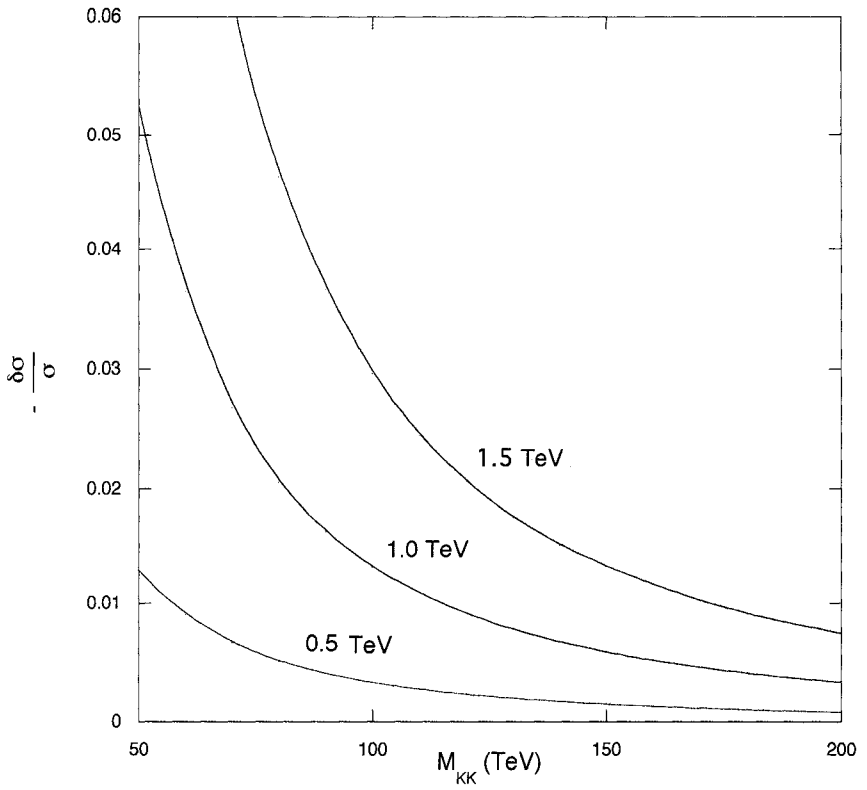

Figure 4.2: Corrections to the top pair production cross-section from the diagrams of Fig. 4.1, as a function of the n = 1 KK gauge boson mass, for center of mass energies of 0.5, 1.0 and 1.5 TeV.

percent sensitivity for $\sqrt{s} = 1$ TeV gives a bound on M_{KK} of 120 TeV.

One can also have the $n = 2, 3, \ldots$ KK gauge bosons exchanged. In universal extra dimensions, the KK gauge boson masses vary linearly with n, and thus one would multiply the result by $\sum_{n=1}^{\infty} \frac{1}{n^2} \sim 1.6$. In the Randall-Sundrum case, one must sum over the zeroes of Bessel functions. Doing this numerically, one also gets approximately an enhancement of 1.6. This would increase the bound by approximately 30 percent, if the model is not cut off at higher scales. Thus, we find sensitivity to masses up to 150 TeV.

Note that there is nothing special about the top quark in this calculation—similar results would occur for production of any fermion pair, including muons. Thus, one could obtain sensitivity to even greater mass scales looking at pair production of other fermions.

One could ask about the reliability of perturbation theory. Because of the enhancement, the effective coupling constants of the weak gauge bosons at the TeV scale are $(8.4)^2 \left(\frac{\alpha_w}{4\pi}\right) \sim 0.20$. Depending on coefficients, there could be significant higher order corrections.

If the fermions are not on the brane, then the electron coupling to the KK gauge bosons will be much weaker since the electron is further away from the TeV brane. Instead of an enhancement factor of 8.4, the coupling decreases [18] by a factor of roughly 5. This change alone would reduce the above bound by a factor of $\sqrt{40}$. In addition, the top quark coupling will be smaller. We consider this bound, as well as other contributions from one-loop corrections, in the next subsection.

4.2.2 Fermions off the brane

As discussed earlier, the scenario in which fermions propagate in the bulk is extremely attractive, in that it provides a simple explanation for the fermion hierarchy. In additon to the tree-level contributions of the last subsection,

there are two additional contributions (these are also present in the on-the-wall case, but are substantially smaller than the tree level contributions). One can calculate one-loop diagrams in which the final state top quarks exchange KK gauge bosons – these can be significant because the gauge bosons can be gluons. The other contribution arises from mixing between the zero mode and KK gauge bosons. We consider each in turn.

Tree-Level Contributions

We first consider the same diagrams as in Fig. 4.1. As noted in the previous paragraph, one expects the bound to be lowered from the on-the-brane case by a factor of at least $\sqrt{40}$, which gives a reach of approximately 25 TeV. This will be lowered further since the top quark is not on-the-brane, and so its coupling will be weakened.

In general, the left- and right-handed top quarks will have different 5-D mass terms, c_L and c_R. This will lead, from Eq. (2.90), to different enhancements for the different chiralities. If the enhancement of the left-handed top quark couplings is α_L, and that of the right-handed top quark couplings is α_R, one can then determine the cross-sections and asymmetries.

Using Godfrey's notation [71] for exchange of a neutral heavy gauge boson

Z', the differential cross-section can be written as

$$\frac{d\sigma_L}{d\cos\theta} = \frac{\pi\alpha^2}{4s}\left\{|C_{LL}|^2(1+\cos\theta)^2 + |C_{LR}|^2(1-\cos\theta)^2\right\} \tag{4.1}$$

where

$$C_{ij} = -Q_f + \frac{C_i^e C_j^t}{c_w^2 s_w^2}\frac{s}{(s-M_Z^2)+i\Gamma_Z M_Z} + \frac{\left(g_{Z'}/g_{Z^0}\right)^2 C_i^{e'} C_j^{t'}}{c_w^2 s_w^2}\frac{s}{(s-M_{Z'}^2)+i\Gamma_{Z'} M_{Z'}}. \tag{4.2}$$

Here, C_i^t are the SM Z^0 couplings and $C_i^{t'}$ are the Z' couplings to the top quark. For right-handed electrons, one substitutes $C_{LL} \to C_{RR}$ and $C_{LR} \to C_{RL}$. From this, one finds the unpolarized total cross-section is given by

$$\sigma = \frac{\pi\alpha^2}{3s}\left[|C_{LL}|^2 + |C_{RL}|^2 + |C_{LR}|^2 + |C_{RR}|^2\right], \tag{4.3}$$

the forward-backward asymmetry is given by

$$A_{FB} = \frac{\left[\int_0^1 - \int_{-1}^0\right] d\cos\theta \frac{d\sigma}{d\cos\theta}}{\left[\int_0^1 + \int_{-1}^0\right] d\cos\theta \frac{d\sigma}{d\cos\theta}}, \tag{4.4}$$

and the left-right asymmetry is

$$A_{LR}^f = \frac{\sigma\left(e_L^-\right) - \sigma\left(e_R^-\right)}{\sigma\left(e_L^-\right) + \sigma\left(e_R^-\right)} \tag{4.5}$$

where σ_L (σ_R) is the cross-section for a left-(right-)handed incoming electron.

Using these results, we find that the corrections to the cross-section, forward-backward asymmetry and left-right asymmetry (using the expected value of -0.2 for the change in the electron coupling to the KK gauge bosons [18]) are given by

$$\begin{aligned} \frac{\delta\sigma}{\sigma} &= (0.24\alpha_L + 0.14\alpha_R)\frac{s}{M_{KK}^2} \\ \delta A_{FB} &= (-0.04\alpha_L - 0.03\alpha_R)\frac{s}{M_{KK}^2} \\ \delta A_{LR} &= (0.26\alpha_L - 0.19\alpha_R)\frac{s}{M_{KK}^2} \end{aligned} \tag{4.6}$$

The results are plotted in Fig. 4.3 as a function of c_L and c_R. Here, we choose $M_{KK} = 10$ TeV, the results in all cases scale like the inverse-square of M_{KK}. These results are for the $n = 1$ KK gauge bosons. Including the sum of all KK modes results in a small change of less than 20 percent (this is less than the sixty percent correction in the last subsection because for some values of the mass term, the couplings of higher modes can be negative).

Depending on how precisely the luminosity at the ILC can be determined, a one-percent measurement of the cross-section is possible, and thus a reach of 10 TeV for much of parameter space can be obtained (and a reach of 15 TeV

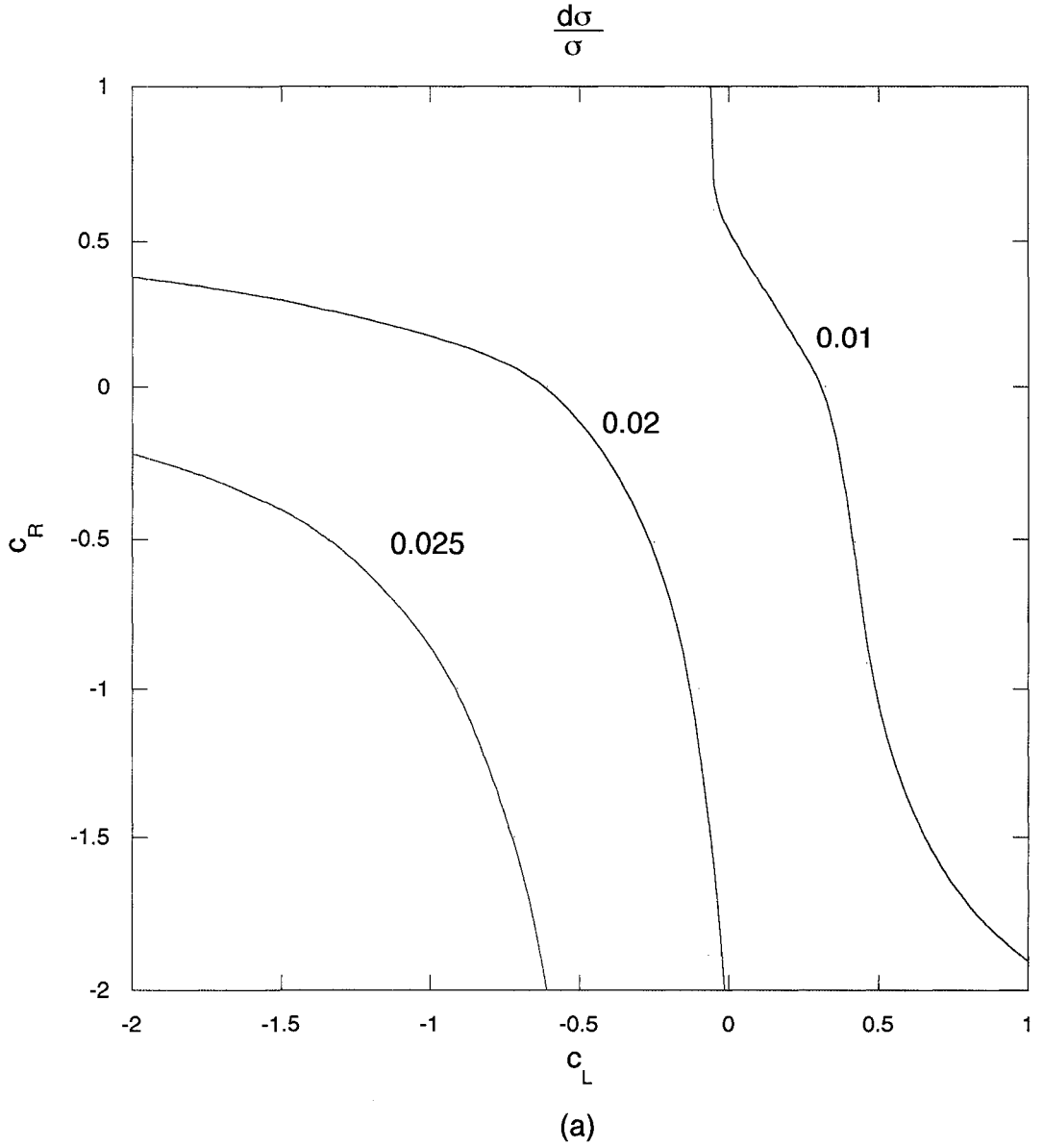

Figure 4.3: Corrections to the SM production cross-section for difference values of c_L and c_R. We have assumed that $M_{KK} = 10$ TeV; the results will scale as $1/M_{KK}^2$.

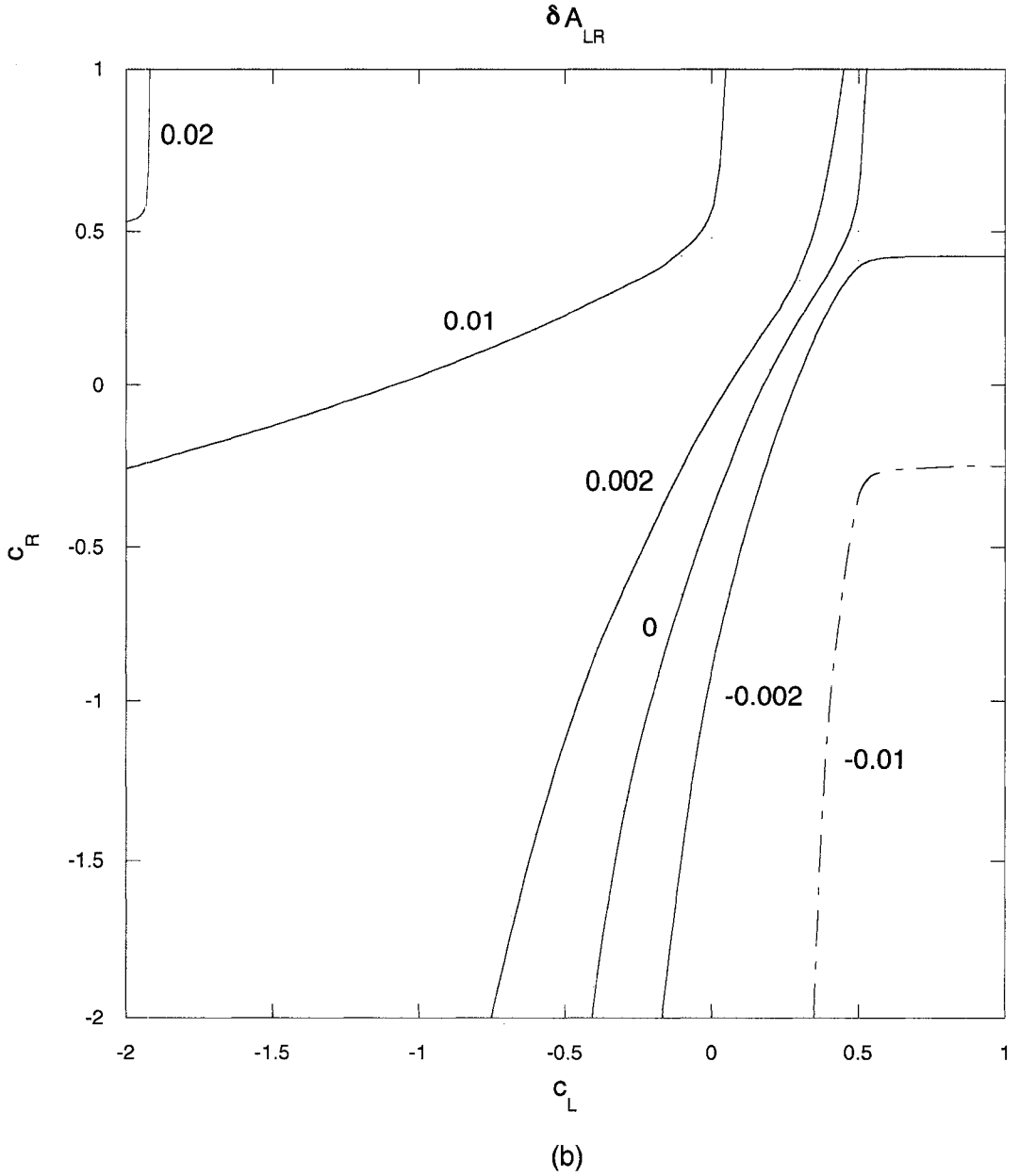

Figure 4.3: Corrections to the SM left-right asymmetry for difference values of c_L and c_R. We have assumed that $M_{KK} = 10$ TeV; the results will scale as $1/M_{KK}^2$.

for some of parameter space is possible). The forward-backward asymmetry is too small to be measurable. The left-right asymmetry is interesting. With a million top pairs expected in several years running, half from left-handed and half from right-handed electrons, assuming 80% polarization, one could reach a sensitivity of approximately 0.002 for A_{LR}, which would also cover most of parameter space, for a 10 TeV KK gauge boson mass, and would cover some of the space even for a 30 TeV mass. It should be noted that the "preferred" range of c_L, c_R, since the right-handed top can be much closer to the TeV brane, is for negative (or near zero) c_R and for c_L positive (but less than 0.5). A clear signature of the model, which could distinguish it from extra-Z models, is the absence of a substantial change in the forward-backward asymmetry.

These bounds could perhaps be improved substantially by including the effects of positron beam polarization and of top quark polarization [71], which can increase the bounds by up to a factor of two. This improvement, of course, depends on the design of the ILC.

One-loop Contributions

We now turn to one-loop corrections to the $\bar{t}t\gamma$ and the $\bar{t}tZ$ vertices. We start with the diagrams in Fig. 4.4. The exchanged KK gauge boson can be either a KK gluon, KK W_3, or a KK B. Of course, one expects the KK gluon to have the biggest effect; this is the KK version of the well-known $\frac{\alpha}{\pi}$ correction to the

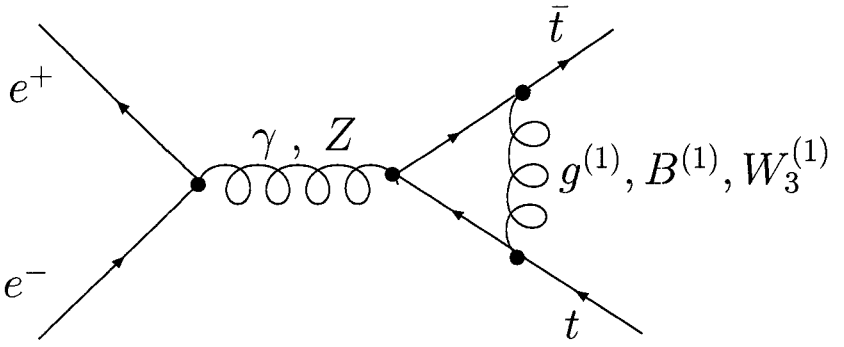

Figure 4.4: The dominant one-loop diagrams affecting top pair production. The exchanged gauge boson is either a KK gluon, KK W_3 or a KK B. Corrections to the electron vertex are negligible since the electron couplings to the KK gauge bosons are suppressed.

value of R in hadron production. In fact, we find this to be the case, but to be complete, we present the results for all of the diagrams.

The most general interactions of the top quark with the γ and Z, assuming massless initial fermions and ignoring the (small) CP-violation, is

$$\Gamma_\mu^V(q^2) = -ie\left[\gamma_\mu(F_{1V}^V(q^2) + \gamma_5 F_{1A}^V(q^2)) + \frac{i\sigma_{\mu\nu}q^\nu}{2m}(iF_{2V}^V(q^2))\right] \tag{4.7}$$

where $V = \gamma, Z$. As calculated in Ref. [72] and discussed by Baur [73], these coefficients can all be bounded at roughly the one percent level. Baur gives the precise bounds that can be obtained at the ILC. However, the bounds that he lists are from early studies [74], where the integrated luminosity is either 100 or 200 fb^{-1}. We are assuming that many years of running at an ILC can yield an integrated luminosity of an inverse attobarn, and thus one can (in the extremely

optimistic case of assuming only statistical uncertainties) scale the results by the square-root of the integrated luminosity ratio for interference diagrams, and the fourth-root for direct terms. Positron polarization (50%) also lowers the limits by 25%, and a center-of-mass energy of 1 TeV also lowers them by a factor of 1.5 [74], compared to the earlier studies which assumed half the center-of-mass energy and no polarization. Including these latter two effects, we take the range of the bounds on the coefficients to be between the values cited by Baur [73] and the optimistic range given with an inverse attobarn luminosity. The ranges of interest are then

$$\begin{aligned} F_{1V}^{\gamma} &: .010 - .024 \\ F_{1A}^{\gamma} &: .003 - .006 \\ F_{2V}^{\gamma} &: .010 - .019 \\ F_{1V}^{Z} &: .003 - .006 \\ F_{1A}^{Z} &: .002 - .006 \\ F_{2V}^{Z} &: .002 - .006 \end{aligned} \tag{4.8}$$

In principle, one could add the effects of these diagrams to the tree-level contribution, and calculate the resulting cross-sections and polarization asymmetries in a unified manner. One could calculate the corrections to the cross-section and asymmetries for a given F; for example, one can show that the

contribution of F_{1V}^Z to $\delta\sigma/\sigma$ is negligible, whereas the contribution of F_{1A}^Z is roughly $\delta\sigma/\sigma = 2.2\,\delta F_{1A}^Z$. However, the tree-level contribution is similar to that of an extra Z boson for which virtually all studies generally refer to cross-sections and asymmetries, while the one-loop contribution involves anomalous γ and Z interactions, for which studies generally refer to the above form factors. Furthermore, the sensitivity to changes in the cross-section and asymmetries were calculated using different assumptions about the collider than those for the sensitivity to changes in the form factors. Since the detailed specifications of the ILC and its detectors are not yet known, we are simply referring to previous studies and thus keep the contributions separate. A more detailed unified study, including top quark and positron polarization asymmetries would be valuable and could make our results more precise.

For a given value of c_L and c_R, we can find the enhancements of the couplings of the left- and right-handed top quarks, determine the value of C and α in the vertex, plug into the expressions, and determine the effect on the six parameters in Eq. (4.7), for $q^2 = s = 1$ TeV^2. As in the tree-level case, including higher order terms will increase the mass reach by approximately 20%—more precision is unnecessary since higher order corrections (such as double KK gluon exchange) will likely have a bigger effect. The results are plotted in Fig. 4.5, assuming $M_{KK} = 5$ TeV. We see that the most sensitive coefficients are the

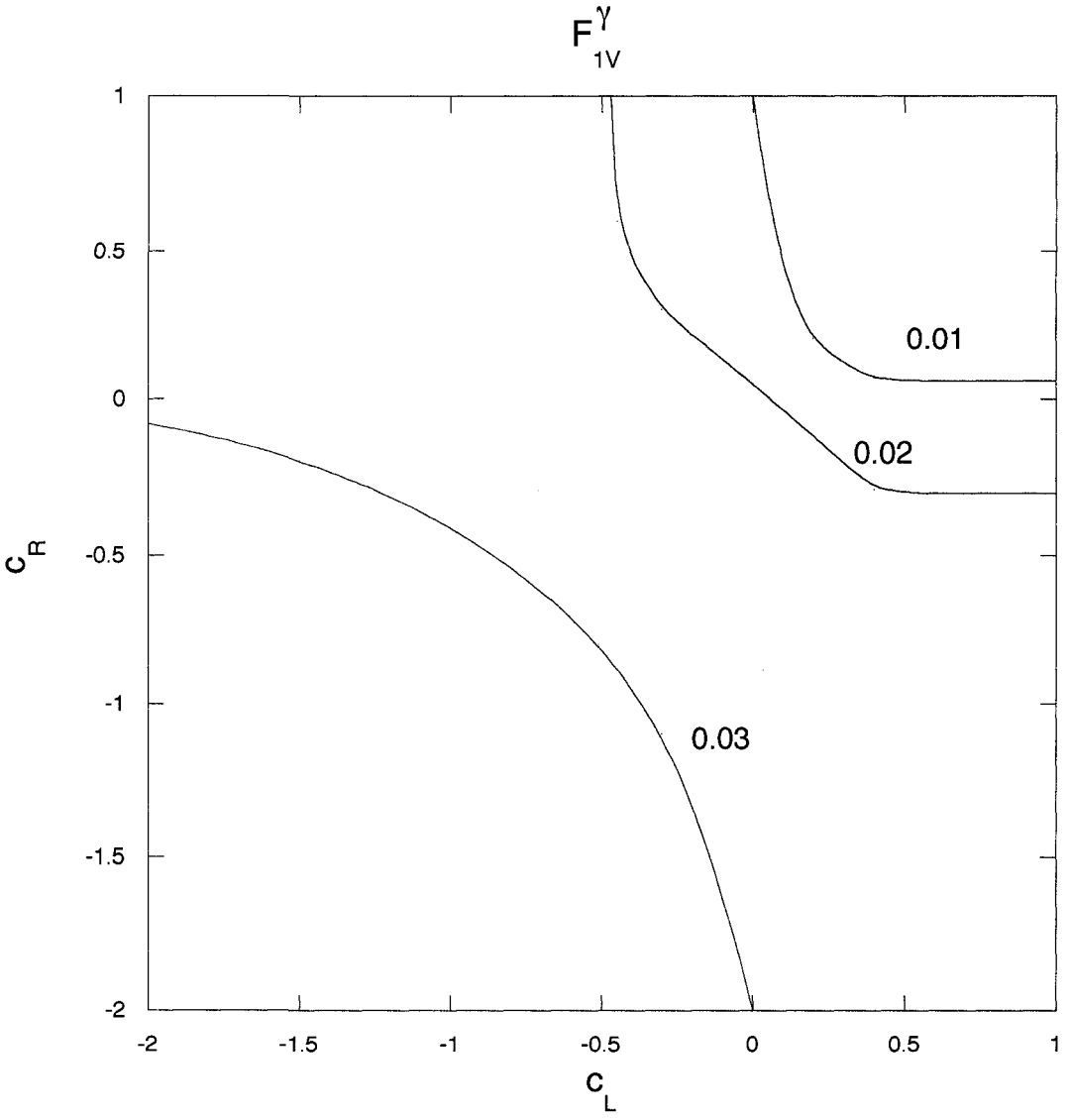

(a)

Figure 4.5: Contributions to the γ and Z form factors as a function of c_L and c_R, for $M_{KK} = 5$ TeV.

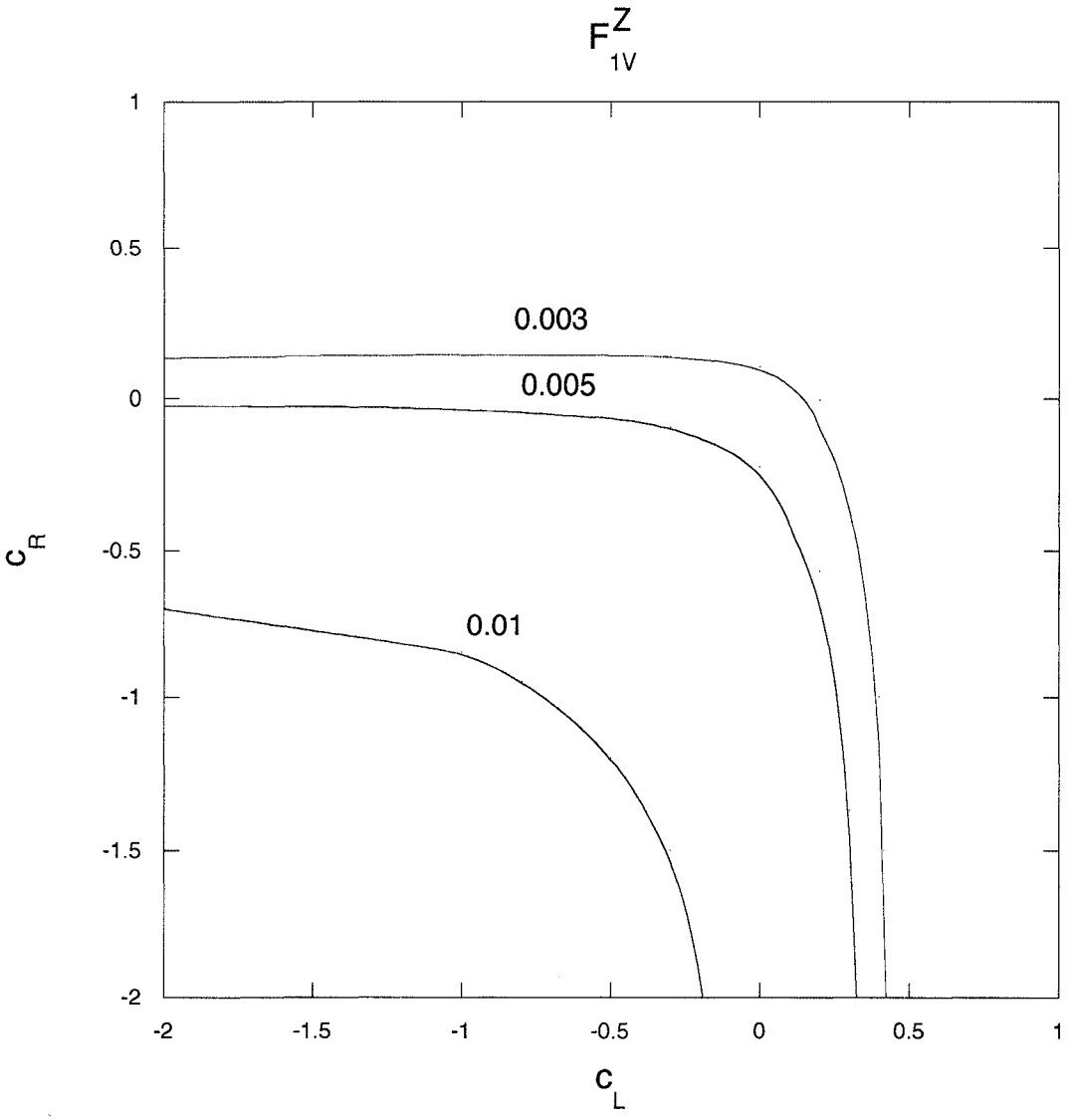

(b)

Figure 4.5: Contributions to the γ and Z form factors as a function of c_L and c_R, for $M_{KK} = 5$ TeV.

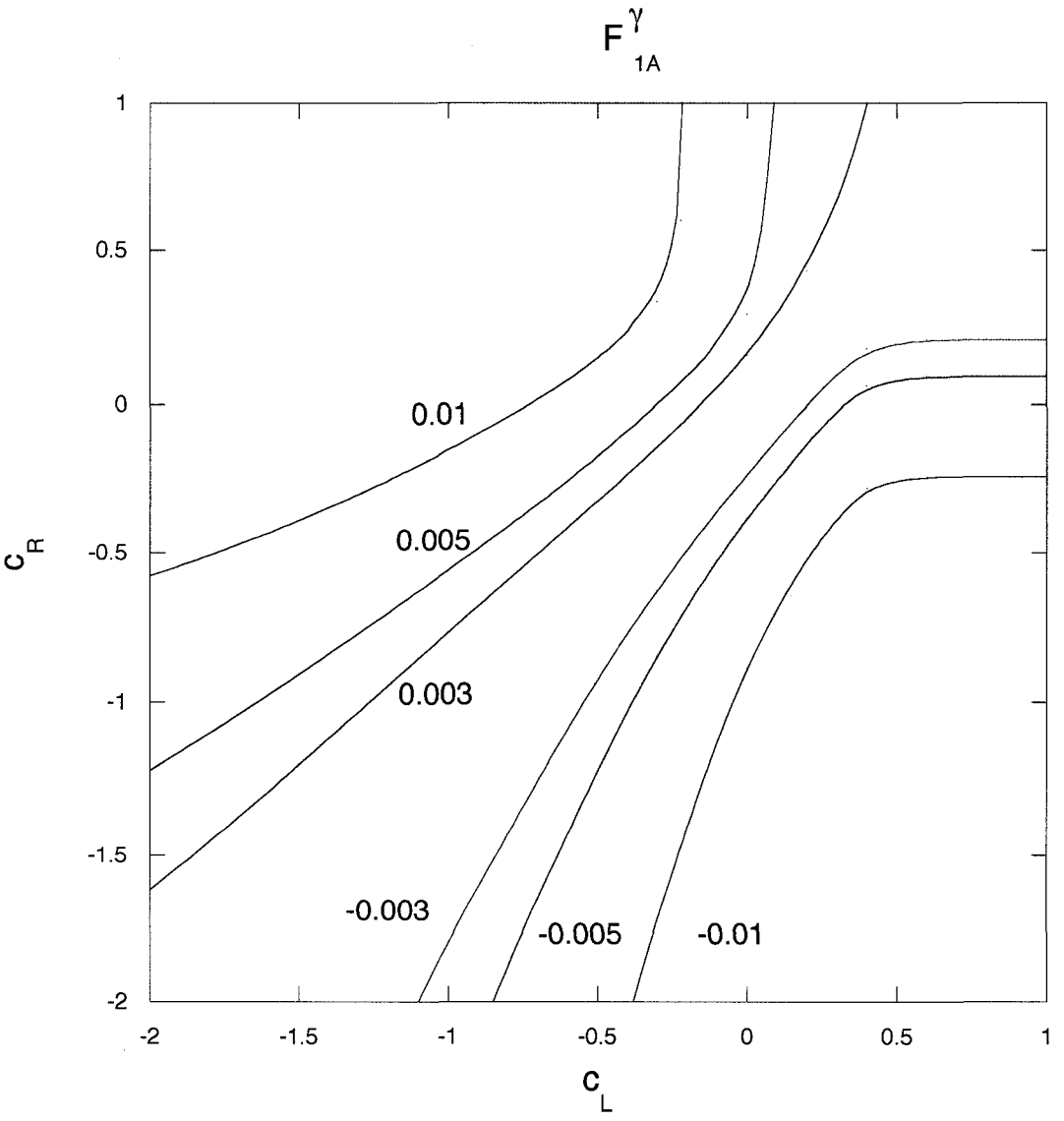

(c)

Figure 4.5: Contributions to the γ and Z form factors as a function of c_L and c_R, for $M_{KK} = 5$ TeV.

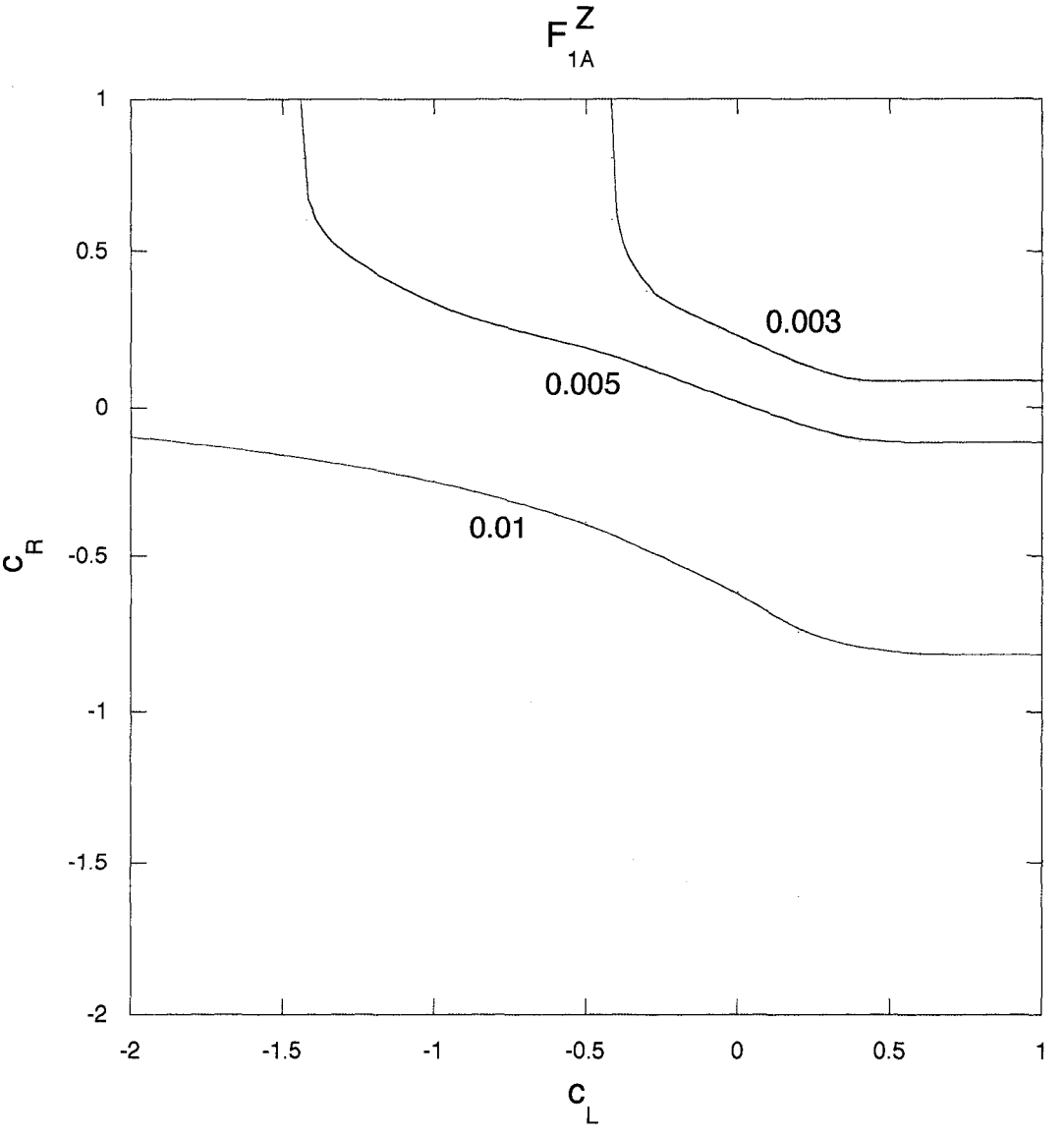

(d)

Figure 4.5: Contributions to the γ and Z form factors as a function of c_L and c_R, for $M_{KK} = 5$ TeV.

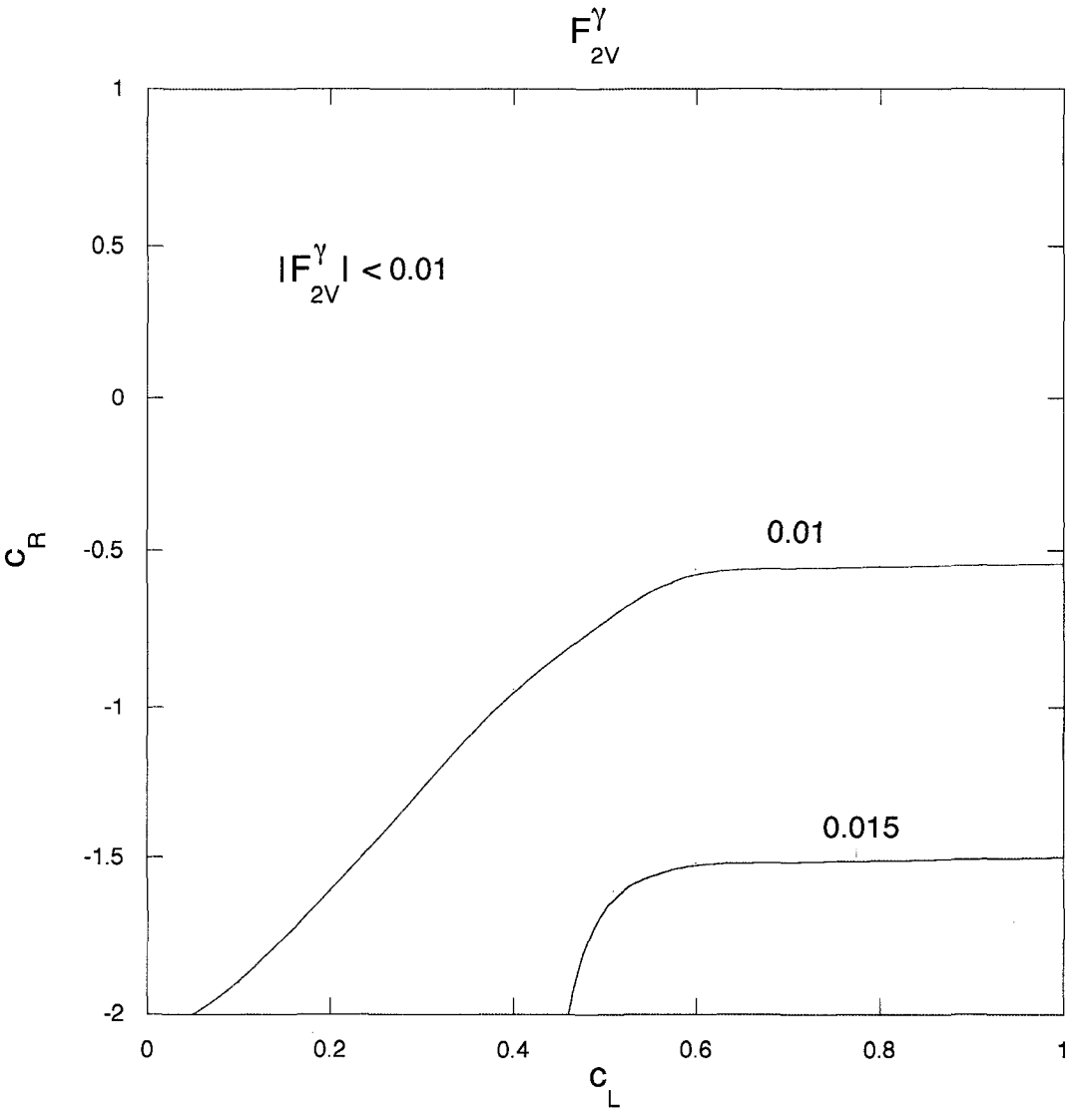

(e)

Figure 4.5: Contributions to the γ and Z form factors as a function of c_L and c_R, for $M_{KK} = 5$ TeV.

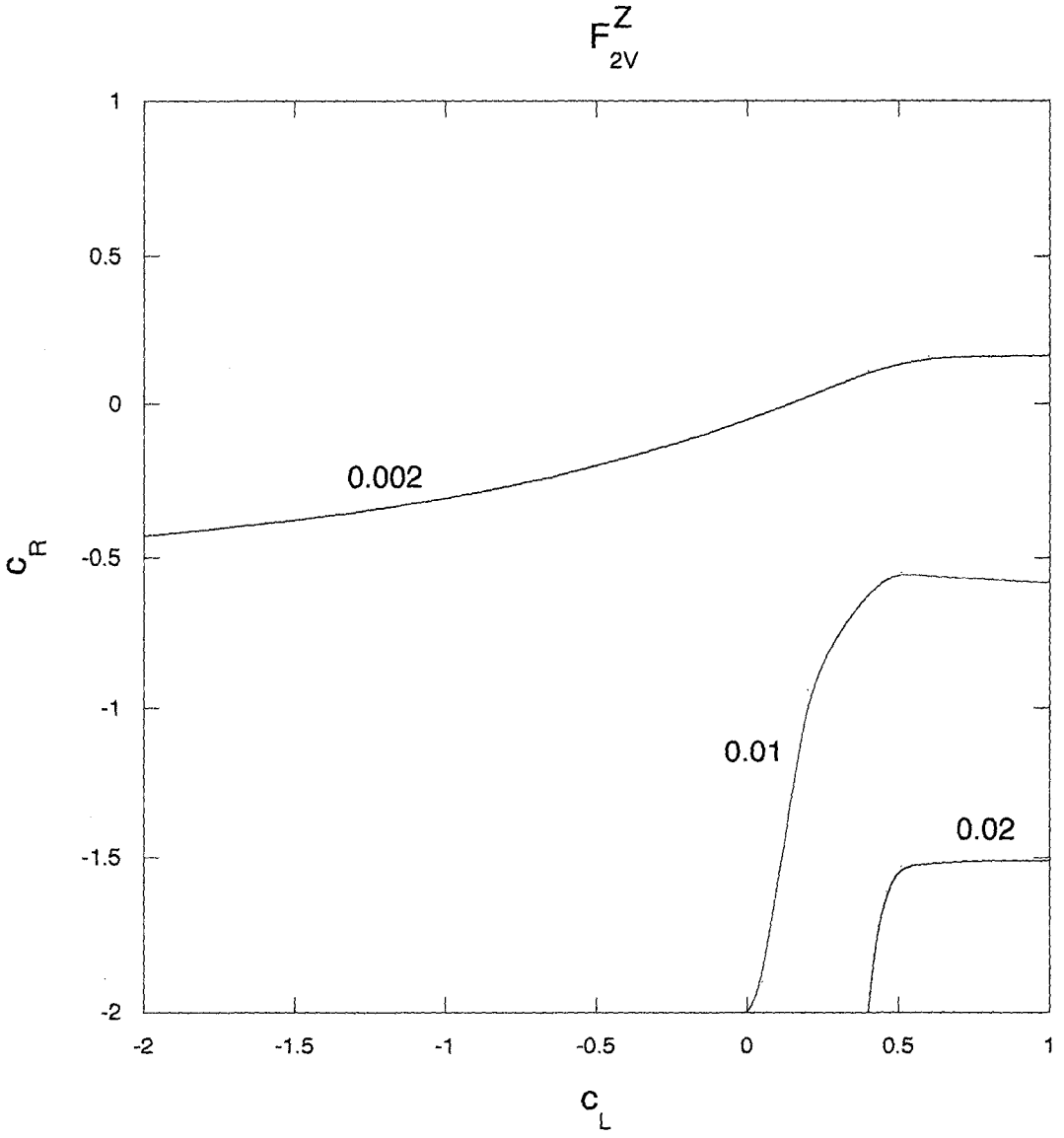

(f)

Figure 4.5: Contributions to the γ and Z form factors as a function of c_L and c_R, for $M_{KK} = 5$ TeV.

couplings of the Z, for which sensitivities to $M_{KK} = 5$ TeV are reached for most of parameter space. However, we have found that for $M_{KK} = 10$ TeV, only a small sliver of parameter space is sensitive. These results are substantially weaker than the results for the tree-level contribution of the last subsection.

Contributions from mixing

The most detailed discussion of top pair production at a linear collider in the Randall-Sundrum model was by Agashe, Delgado, May and Sundrum (ADMS) [64], which was recently summarized by Agashe [75]. They discussed the contributions from the mixing between the Z and the KK Z bosons. This mixing occurs from the Higgs vacuum expectation value. The biggest effect is on the right-handed top quark coupling, and they find that

$$\frac{\delta(g_Z^{t_R})}{g_Z^{t_R}} \sim \frac{m_Z^2}{(0.41 M_{KK})^2} \frac{1-2c_R}{3-2c_R} \left(\frac{-k\pi R}{2} + \frac{5-2c_R}{4(3-2c_R)} \right) \tag{4.9}$$

It is straightforward to convert this into a shift in F_{1V}^Z and F_{1A}^Z,

$$F_{1V}^Z = F_{1A}^Z = -\frac{\tan\theta_W}{3} \frac{\delta(g_Z^{t_R})}{g_Z^{t_R}} \tag{4.10}$$

For a KK gauge boson mass of 5 TeV, this gives a result for F_{1V}^Z and F_{1A}^Z which ranges from 0 at $c_R = 1/2$, to 0.002 at $c_R = 0$, to 0.004 at $c_R = -0.2$.

We see that the 5 TeV mass scale can barely be reached for the $c_R < 0$ part of parameter space, and thus could have a greater reach than the one-loop contributions for some of the parameter space. But it is substantially weaker than the tree-level contribution. As we will see in the next section, however, the effects of mixing between the top quark and the KK top can be substantially larger, and could be competitive with the tree-level contribution.

4.3 Effects of KK Fermions and Brane Kinetic Terms

In this analysis, we have only included the effects of KK gauge bosons. As noted in Section 4.2, the masses of the KK gauge bosons are related to the zeroes of Bessel functions of order 1, while the masses of the KK fermions are related to zeroes of Bessel functions of order $|c \pm 1/2|$. In the absence of brane kinetic terms, the masses of the KK tops are thus related to those of KK gauge bosons, and their effects must be considered. In particular, the masses of the left-handed KK tops [64, 75] are given by $m_{t_L^n} \sim \pi k e^{-k\pi r_c}(n - c_L/2) \sim 1.28 m_{KK}(n - c_L/2)$, where m_{KK} is the $n = 1$ KK gauge boson mass[1]. For $n = 1$ and $c_L = 0.4$, this gives virtually equal $n = 1$ KK top and KK gauge

[1]In [75], there are two typographical errors in Eq. (16): the factor of $\sqrt{1/2 - c_L}$ should be in the denominator and the factor of 0.78 should be 1/0.78. There are purely typographical and do not affect the results.

boson masses.

Clearly, the results from tree-level KK gauge boson exchange will not be affected, except for small mixing effects, by KK top contributions. There will, however, be contributions to the one-loop diagrams of Fig. 4.4, in which the internal top quark lines are replaced by KK top quark lines. We have calculated the effects of these contributions, and find them to be smaller, in all cases, than the previous results.

A much bigger effect arises from mixing between the top quark and the KK top quark. This arises from mixing of the zero-mode t_R with the KK t_L through the Higgs vev, and is discussed in detail by Agashe [75]. Using Eq. (4.10), Agashe's result can be written as

$$\delta F_{1V}^{Z} = F_{1A}^{Z} \sim \sum_{n} \frac{-1}{2 \sin 2\theta_W} \left(\frac{m_t}{m_{t_L^{(n)}}} \right)^2 \left(\frac{1 - e^{-2k\pi R(1/2 - c_L)}}{1/2 - c_L} \right). \qquad (4.11)$$

This is plotted as a function of c_L for several masses in Fig. 4.6, where the sum over the KK modes has been included. The range $c_L > 0.5$ is exceeedingly disfavored, since the Yukawa coupling of the top quark would then be exponentially suppressed. We see that for $c_L = 0.4$, a reach of 10 TeV is barely possible, with the optimistic assumptions discussed earlier for the reach of the ILC. For c_L very close to 0.5, however, the reach can exceed that of the tree-level KK gauge boson exchange.

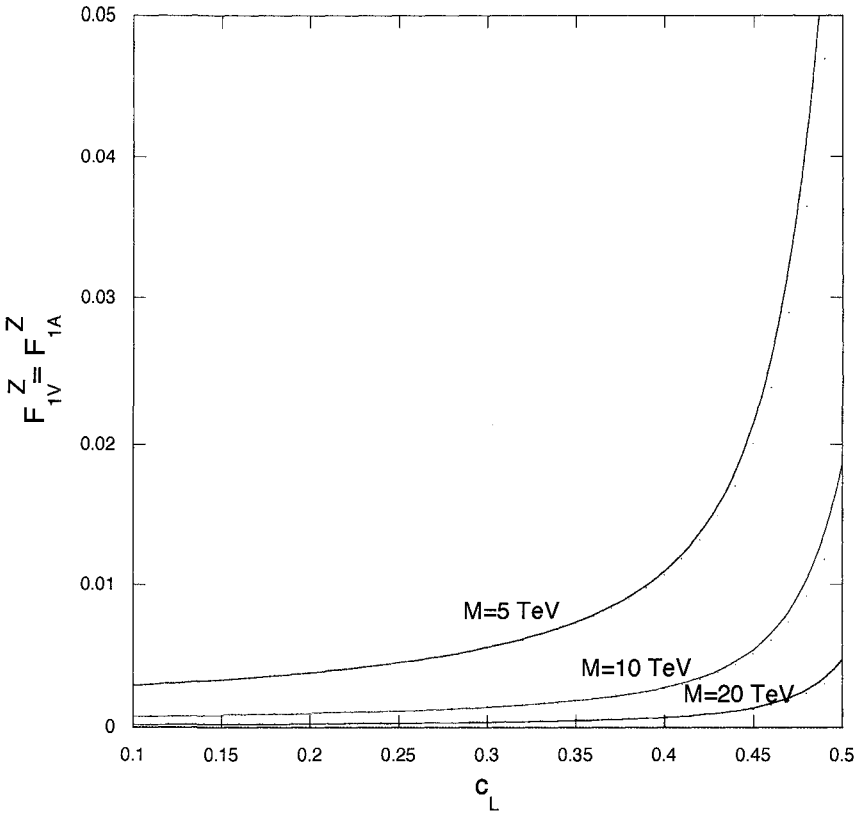

Figure 4.6: Effects on the Z form factors due to top/KK top mixing as a function of c_L for various values of the KK mass. A high luminosity ILC should have a sensitivity of 0.006 to these form factors, and could optimistically reach 0.003.

Thus, mixing can give a reach which can be larger than that of the tree-level KK gauge boson exchange, but only in the upper end of the $0.4 \leq c_L \leq 0.5$ range. Although this seems narrow, it is a particularly interesting range of c_L. If c_L were larger, the Yukawa coupling would be suppressed and the top mass would be too small, and if it were much smaller, there might be dangerous contributions to the $\bar{b}bZ$ vertex. A word of caution is that the large mixing can cause problems with precision electroweak fits, although a custodial SU(2)

symmetry or brane kinetic terms can ameliorate the problems (if there is a custodial SU(2) symmetry, one should include effects of the Z' as well). Mixing contributions between the zero-mode t_L and the KK t_R are expected to be small since c_R is not expected to be in this range. Note that a clear signature of the dominance of mixing would be the equality of the contributions to F_{1V}^Z and F_{1A}^Z. Here, one looks for deviations in the right-handed top quark couplings, and this might require determination of the top quark polarization. Previous analyses have looked at F_{1V}^Z and F_{1A}^Z separately (assuming one is nonzero and all others vanish) – here a more unified analysis for the ILC would be welcomed.

Finally, we consider the effects of brane kinetic terms (BKTs). A detailed discussion of these terms in flat space can be found in [66, 67, 68]. In the context of Randall-Sundrum models, two papers by Carena, Delgado, Ponton, Tait and Wagner (CDPTW) [61, 62] have extensively studied BKTs and their effects on phenomenology. The BKTs for fermions arise in the 5D action

$$S = -\int d^4x \int_0^{\pi R} dy \sqrt{-G} \left(i\bar{\Psi}\Gamma^A e_A^M D_M \Psi + im(y)\bar{\Psi}\Psi + 2\alpha_f \delta(y-\pi R)\bar{\Psi}_L \gamma^a e_a^\mu \partial_\mu \Psi_L \right) \quad (4.12)$$

where Γ and γ are the 5D and 4D Dirac matrices, and the last term is the BKT. Here, the δ function is normalized so that $\int_0^{\pi R} 2\delta(y)dy = 1$. The coefficient, α_f, has dimensions of length. Note that this is an IR-brane BKT, whereas a

UV brane BKT would be proportional to $\delta(y)$, but one expects the UV brane BKTs to be less phenomenologically relevant. More details can be found in CDPTW.

One can also have gauge field BKTs. For a $U(1)$ gauge group, the relevant part of the action is

$$S = -\int d^4x \int_0^{\pi R} dy \frac{1}{2} B_\mu \mathcal{O}^{\mu\nu} B_\nu \tag{4.13}$$

where

$$\mathcal{O}^{\mu\nu} = \frac{1}{g_5^2}\left(P^{\mu\nu} + \eta^{\mu\nu}\partial_y(e^{-2\sigma}\partial_y) + 2\delta(y) r_{UV} P^{\mu\nu} + 2\delta(y-\pi R) r_{IR} P^{\mu\nu}\right) \tag{4.14}$$

and $P^{\mu\nu} \equiv \eta^{\mu\nu}\partial^2 - \partial^\mu\partial^\nu$. Note that we have explicitly included both UV and IR BKTs.

CDPTW [61, 62] use these actions and find all of the KK masses, wavefunctions and couplings in the model, and the reader is referred to those papers for the full expressions. They find that the IR BKTs repel the KK wavefunctions from the IR brane, thus reducing the couplings of the zero-mode fermions to the KK gauge bosons. As a result, the effects on precision tests is reduced, and KK masses of the order of a few TeV (and thus in reach of the LHC) become allowed. In addition, BKTs can also make the model more compatible with

grand unification. Relatively large BKTs (of order πR) are needed to have a substantial impact, but such terms are not unnatural.

As discussed in the Introduction, our approach in this paper is to consider KK masses which are out of reach of the LHC. The effect of the BKTs discussed by CDPTW is then to reduce the coupling of fermons to KK gauge bosons, and thus lower the effects in top pair production. In short, we have added some parameters to the model which, if large enough, can substantially weaken our bounds.

One interesting feature concerns the conformal limit ($c_L = c_R = 1/2$). At this point, without BKTs, the coupling of the zero mode fermions to the KK gauge bosons vanish, and all of the contributions we discussed (involving KK gauge bosons) vanish (as well as many contributions to electroweak precision tests). This is because the fermion zero-mode wavefuntion is flat, and thus proportional to the gauge zero-mode wavefunction, which is orthogonal to the KK gauge boson wavefunctions. This was first noticed in the Randall-Sundrum model in Ref. [64], and for Higgsless models in Ref. [76]. With BKTs however, unless the gauge and fermion BKTs are identical, the fermion and gauge boson orthogonality conditions will differ, and the couplings will not vanish in the conformal limit. Whether the couplings are large enough to make a measureable contribution depends, of course, on the size of the BKTs.

4.4 Discussion and Conclusions

The Randall-Sundrum model is one of the most promising approaches to solving the gauge hierarchy problem. The five-dimensional spacetime compactified on an orbifold, with a slice of AdS_5 describing the bulk geometry, cannot only explain a large hierarchy but also may naturally arise from string theory. The original form of the model had all of the Standard Model particles on the TeV brane, but there has been much interest in versions of the model in which gauge bosons and/or fermions can propagate. Such models can also naturally explain the fermion mass hierarchy. In this case, the KK excitations of the gauge bosons and/or fermions can have significant phenomenological consequences.

Most analyses of the phenomenology of the Randall-Sundrum models have looked at the effects of the KK excitations on precision electroweak constraints, and there have been many interesting modifications to the model which ameliorate many of these constraints. This can allow the KK excitations to be within reach of the LHC. The most appealing of these modifications include imposing a custodial $SU(2)$ gauge symmetry in the bulk (which may come from a global $SU(2)$ symmetry in the AdS/CFT related conformal theory), or by adding gauge or fermion brane kinetic terms, or both.

Our approach is different. We will suppose that the KK excitations have masses well in excess of 5 TeV, and are thus out of range of the LHC. We

also do not concern ourselves with precision electroweak constraints (which may still be signficant in the $5 - 15$ TeV mass range), assuming that one of the modifications discussed above can ameliorate the constraints, if necessary. We have argued that top pair production could be the first signature of these excitations, since the top quark, due to its large mass, must be close to the TeV brane. Thus, it will feel the effects of these excitations more strongly than other fermions.

We have calculated top pair production at the ILC in the Randall-Sundrum model. Note that in many versions of the model, such as the version with a custodial $SU(2)$ symmetry or versions with extended gauge or fermion sectors, there will be additional fields which could affect top pair production. Unless there is destructive interference plus some tuning; however, such fields are likely to increase the bounds. For simplicity, we have only considered the KK excitations of Standard Model particles.

When all fermions are on the TeV brane, direct KK gauge boson exchange gives a sensitivity to KK gauge boson masses up to 150 TeV. The most attractive models, though, are those in which fermions propagate in the bulk. In this case, the tree-level KK gauge boson exchange diagram still dominates for much of parameter-space, but the reach is much smaller, since the electron coupling is much weaker. We found the change in the cross-section and left-right asym-

metry as a function of the fermion mass paramters and the KK gauge boson mass, and obtained a sensitivity to KK gauge boson masses of approximately 10-20 TeV, depending on the mass parameters.

We then considered the one-loop diagrams in which KK gauge bosons are exchanged by the top quarks in the final state. The dominant diagram is due to KK gluon exchange. These will affect the γ and Z form factors, and we find sensitivity in much of parameter-space to 5 TeV KK gauge boson masses, but 10 TeV masses are out of reach. The effects of KK fermions on these results is small.

Finally, mixing between the top quarks and the KK tops can be substantial in the narrow window in which c_L is between 0.3 and 0.5. Although this window is narrow, it is in the phenomenologically preferred range. The reach can exceed 10 TeV for some of this range.

A more detailed phenomenological analysis is needed. Effects of positron polarization and top quark polarization have not been included. Further, the experimental sensitivities to the various form factors were determined by assuming that only one was nonzero and the relationship between those form factors and experimentally observed quantities is unclear (in view of the different assumptions made). The basic version of the Randall-Sundrum model has only three parameters – c_L, c_R and M_{KK}, with brane kinetic terms playing

a role if they are sufficiently large. This is a sufficiently small parameter set that an event generator could be constructed. Recently, a version of Pythia for Universal Extra Dimensions [77] was developed; such a tool could be developed for this model. Certainly, one expects models with Kaluza-Klein excitations to behave in some sense like extra Z models (as in tree-level exchange), and in some sense like anomalous gauge boson couplings (as in the one-loop diagrams and in mixing), so a Pythia-type gnerator would be helpful.

Chapter 5

Heavy Charged Leptons

In Chapter 2 we discussed the possibility of a sequential, non-degenerate fourth generation of matter. In this Chapter, we will investigate the ability of the Large Hadron Collider (LHC) and the International Linear Collider (ILC) to detect the production of the fourth generation charged lepton, L. Although the detection of heavy quarks, U and D, and heavy neutrinos N have been studied, relatively little work has considered heavy charged lepton detection.

The heavy quarks should be relatively straightforward to detect at the LHC. However, L signatures will have a substantially lower rates and larger backgrounds then the heavy quarks. This limits the heavy lepton mass values that be probed. In section 5.1 we will address heavy charged lepton production and detection at the Large Hadron Collider.

The lower center of mass energy at the ILC will limit the mass of heavy

lepton pair production. Single heavy lepton production is the only way to see heavy leptons above 250 GeV at the International Linear Collider, which we will investigate in section 5.2.

5.1 Large Hadron Collider

The primary mechanisms for heavy charged lepton production at the Large Hadron Collider (LHC) are gluon fusion and quark-antiquark annihilation. See Fig. 5.1 for the associated Feynman diagrams. In the following calculations, we use the unitary gauge so we do not need to include the Goldstone bosons.

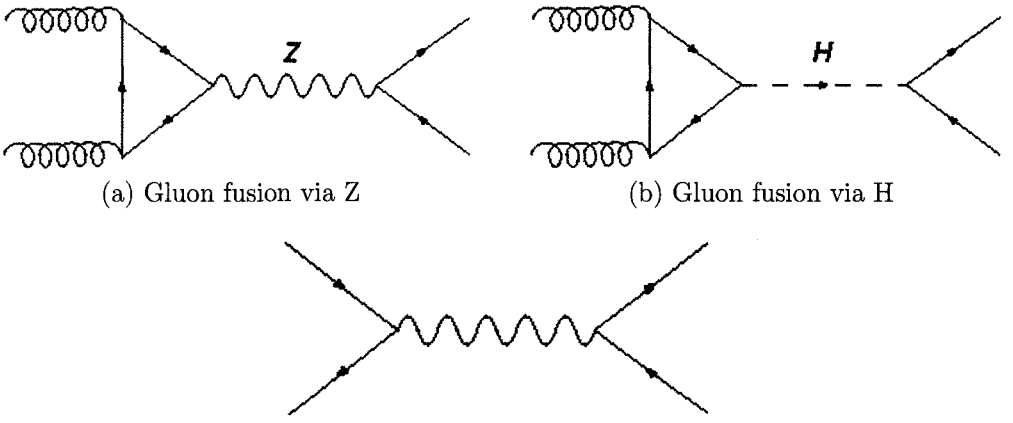

(a) Gluon fusion via Z

(b) Gluon fusion via H

(c) Quark-antiquark annihilation

Figure 5.1: Feynman diagrams for heavy lepton production at the Large Hadron Collider: (a) and (b) gluon fusion through a quark loop and a Z or Higgs intermediate boson to produce a heavy lepton pair and (c) quark-antiquark annihilation $q\bar{q} \to \gamma^*, Z^* \to L\bar{L}$.

The production processes from Fig. 5.1 lead to the following partonic cross-sections [37] where s is the center-of-mass energy at the partonic level, α_s is

the strong coupling:

- From Fig. 5.1a, the cross-section of gluon fusion with an intermediate Z boson is

$$\sigma(gg \to Z \to L^- L^+) = \frac{\alpha^2 \alpha_s^2 m_L^2}{2048\pi \sin^4\theta_W M_W^4} \sqrt{1 - 4\frac{m_L^2}{s}}\, |I|^2 \tag{5.1}$$

where

$$I = 2\sum_q (\pm) \int_0^1 dx \int_0^{1-x} dy \, \frac{xy}{xy - m_q^2/\hat{s}} \tag{5.2}$$

with q summing over the quark flavors. The $(+)$ corresponds with isospin $+\frac{1}{2}$ quarks (u, c, t) and the $(-)$ corresponds with the isospin $-\frac{1}{2}$ quarks (d, s, b).

- From Fig. 5.1b, the cross-section of gluon fusion with an intermediate Higgs boson of mass μ is

$$\sigma(gg \to H \to L^- L^+) = \frac{\alpha^2 \alpha_s^2 m_L^2}{4608\pi \sin^4\theta_W M_W^4} \left(1 - 4\frac{m_L^2}{\hat{s}}\right)^{3/2} \frac{\hat{s}^2}{(\hat{s} - \mu^2)^2 + \Gamma_H^2 \mu^2} |J|^2 \tag{5.3}$$

where

$$J = 3\sum_q \int_0^1 dx \int_0^{1-x} dy \, \frac{1 - 4xy}{1 - xy\,\hat{s}/m_q^2} \tag{5.4}$$

- From Fig. 5.1c, the cross-section of quark-antiquark annihilation with intermediate virtual photon and Z boson is

$$\sigma(q\bar{q} \to \gamma^*, Z^* \to L^- L^+) =$$

$$\frac{8\pi\alpha^2}{9}\left[\begin{array}{l}\sqrt{1-4\frac{m_L^2}{s}}\left(1+2\frac{m_L^2}{s}\right) \\ \quad \cdot\left(\frac{e_i^2}{s}-\frac{e_i(L_q+R_q)(L_e+R_e)}{8\sin^2\theta_W\cos^2_W}\frac{(s-M_z^2)}{(s-M_Z^2)^2+\Gamma_Z^2M_Z^2}\right) \\ +\frac{(L_e^2+R_e^2)}{128\sin^4\theta_W\cos^4\theta_W}s\sqrt{1-4\frac{m_L^2}{s}} \\ \quad \cdot\frac{\left(1+2\frac{m_L^2}{s}\right)(L_q+R_q)^2+\left(1-4\frac{m_L^2}{s}\right)(L_q-R_q)^2}{(s-M_Z^2)^2+\Gamma_Z^2M_Z^2}\end{array}\right] \tag{5.5}$$

where e_i is the charge of quark i, $L_e = 2\sin^2\theta_W - 1$, $R_e = 2\sin^2\theta_W$, $L_q = \tau_3 - 2e_i\sin^2\theta_W$, $R_q = -2e_i\sin^2\theta_W$ with $\tau_3 = 1(-1)$ if $e_i = \frac{2}{3}(-\frac{1}{3})$.

Integrating the partonic cross-sections over the following parton distribution functions [48] using the EHLQ parameterization [78]

$$xg(x) = (2.62 + 9.17x)(1-x)^{5.9} \tag{5.6}$$

$$xu_v(x) = 1.78x^{0.5}(1-x^{1.51})^{3.5} \tag{5.7}$$

$$xd_v(x) = 0.67x^{0.4}(1-x^{1.51})^{4.5} \tag{5.8}$$

yields the cross-section displayed in Fig. 5.2.

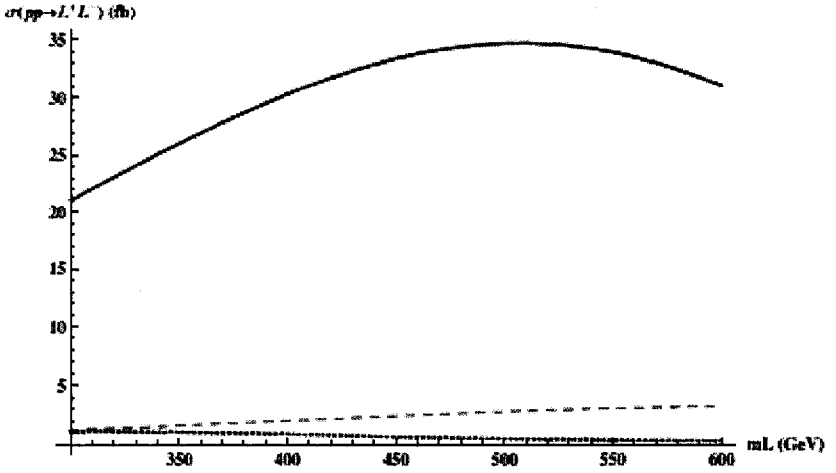

Figure 5.2: The contributions to the $pp \to L^- L^+$ cross-section (in femtobarns) as a function of the heavy lepton mass m_L and integrated over the parton distributions in the sequential SM framework. The dotted line is the quark-antiquark annihilation. The dashed line is the gluon fusion via the Z boson and the solid line is the gluon fusion via the Higgs.

The heavy lepton generally decays into a W boson and missing energy (carried off by a neutrino). Typical cross-sections are ~ 30 fb. Since the LHC will have a luminosity of 10^{34} cm^{-2} s^{-1}, the event rate for heavy lepton pair production is ~ 15 events/week. The W bosons decay primarily into hadrons which will be difficult to distinguish from the hadrons from numerous other processes. The W also decays to lepton-neutrino pairs. To reconstruct the heavy lepton pairs, one could look for electron-muon pairs with missing energy, but this only occurs for $\frac{2}{81}$ of the events. This means there will be only 15 events per year on top of the normal WW pair decays.

In Ref. [79], Hinchliffe *et al.* devised some cuts to remove the WW background. By requiring the angle between the leptons be > 2 radians, the back-

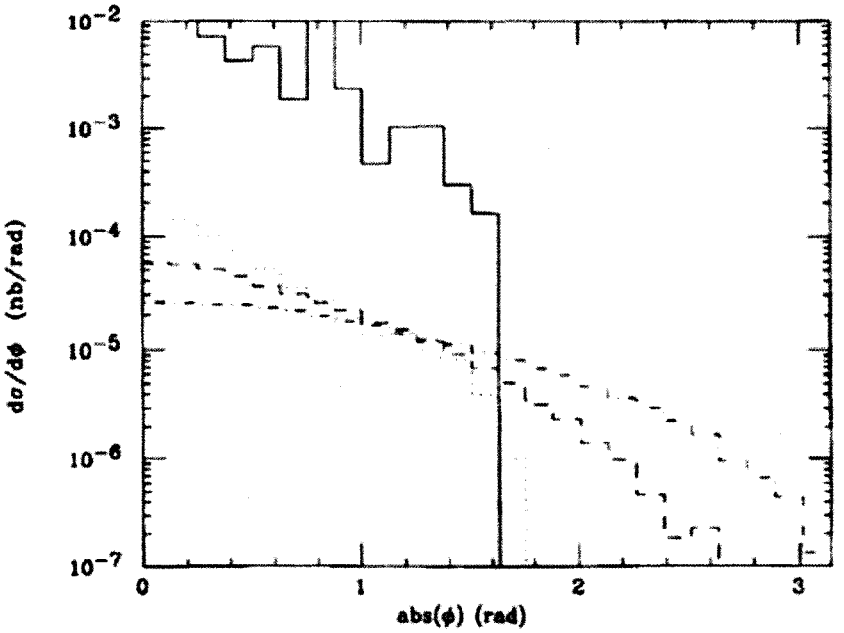

Figure 5.3: The differential cross-section with respect to ϕ, the azimuthal angle for the process $pp \to L^- L^+ + X \to \ell^{\pm} W^{\mp} (\to hadrons) N \bar{N} \nu + X$ at $\sqrt{s} = 40$ TeV. N is assumed to be massless. The solid line is the background, while the dotted, dashed, and dot-dashed lines correspond to $m_L = 100, 200$ and 400 GeV [79].

ground was eliminated and some events remained, see Fig. 5.3. At the SSC, with $m_L = 400$ GeV, they found 3 events/year with no background. Although the LHC has a lower center-of-mass energy than the SSC, the increased luminosity of the LHC will result in a similar event rate at large azimuthal angles.

Due to the low event rates and large backgrounds, it will difficult, if not impossible, to detected heavy charged leptons at the LHC. The ability to detect the heavy lepton pairs will be determined by the accuracy of the background and the Monte Carlo simulations. Further work is needed to be certain.

5.2 International Linear Collider

At the International Linear Collider (ILC), heavy leptons can be easily produced and detected up to the kinematic limit. However, the initial stage of the ILC will probably be at a center of mass energy of 500 GeV, in which case pair production of heavy leptons with masses above 250 GeV will not be possible. The only possible production mechanism would be through single L production, in association with a lighter Standard Model charged lepton. Since mixing between L and μ or e is expected to be small, we will focus on the process $e^+e^- \to L\tau$, which can occur through a nonzero θ_{34} mixing angle. Although single production of heavy charged leptons has been studied before [21, 22, 23, 24, 25], all of these studies considered vectorlike or mirrorlike leptons, and we know of no calculations of this process with a heavy neutrino at a linear collider. An analysis of sequential heavy charged leptons in Z-decays [80] ignored the mass of the heavy neutrino.

In the following subsection, 5.2.1, we present the relevant diagrams in the sequential Standard Model and calculate the cross-section as a function of the N and L masses. Subsection 5.2.2 considers the cross-section in the two Higgs doublet model and in the Randall-Sundrum model. Finally, in Subsection 5.2.3, we discuss detection possibilities and present our conclusions.

5.2.1 Sequential Standard Model

A single charged heavy lepton can only be produced if the fourth generation mixes with the lighter generations. Bounds on the mixing angle θ_{34} arise from observation of universality in τ decays; a nonzero mixing angle would multiple the rate by $\cos^2\theta_{34}$. This was analyzed by Swain and Taylor [81] who found a model-independent bound of $\sin^2\theta_{34} < 0.007$. This is a particularly interesting value. If one diagonalizes a seesaw-like 2×2 mass matrix for the τ and L, one expects $\sin^2\theta_{34} \sim m_\tau/m_L$, which gives 0.007 for an L mass of 250 GeV. We will assume this value of the mixing angle in our numerical results, and can easily scale the cross-section for smaller mixing angles.

The diagrams are listed in Fig. 5.4 and grouped as the self energy, vertex and box type contributions. We use the 't-Hooft-Feynman gauge throughout, and thus charged Goldstone bosons, G, must be included. Note that the electron-Higgs couplings are neglected due to small Yukawa couplings. The internal neutrino lines get a contribution from each of the four neutrinos, and thus each diagram is proportional to $V_{4i}^* V_{i3}$. When summing over the four neutrinos, parts of the matrix elements that are independent of the neutrino mass will cancel by unitarity of the 4-D CKM-like matrix. This causes the ultraviolet divergences to cancel in the sum over neutrinos.

The calculation of the cross-section is performed by using the `FeynArts`,

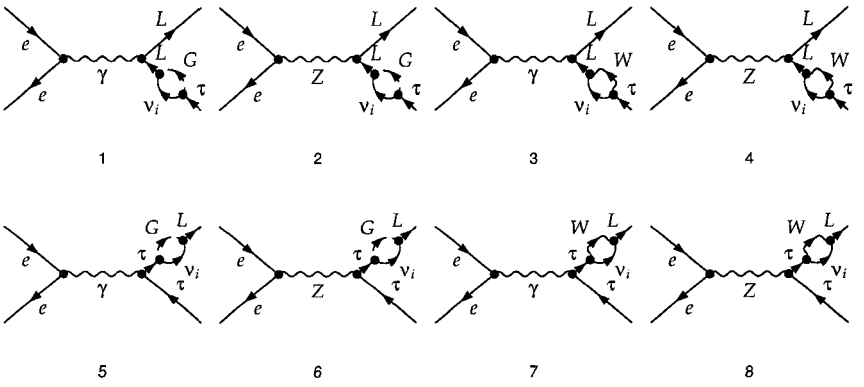

(a) The leading order self energy contributions

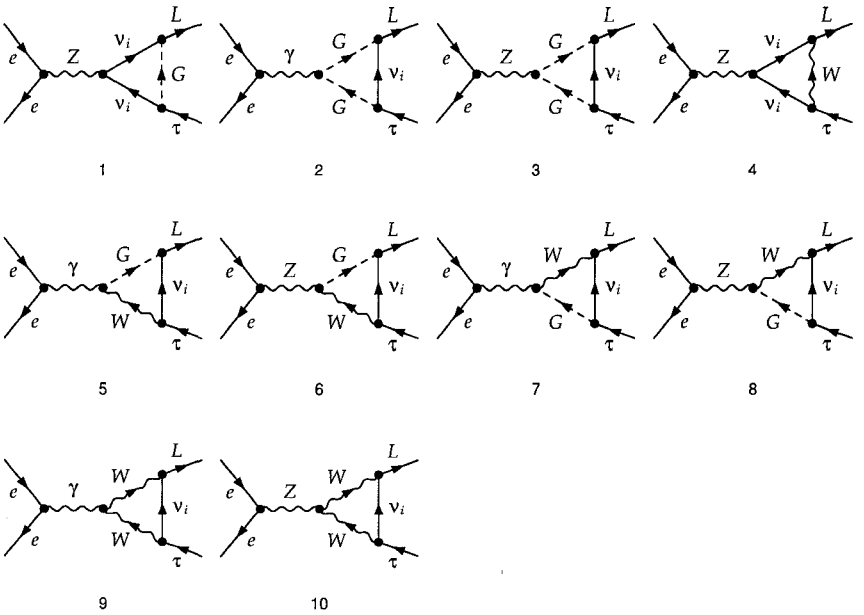

(b) The leading order vertex contributions

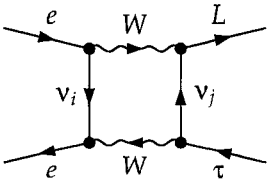

(c) The leading order box contributions

Figure 5.4: The leading order contributions to the $e^+e^- \to L\bar{\tau}$ process in the sequential SM. The 't-Hooft-Feynman gauge is assumed and the light electron-Higgs couplings are neglected.

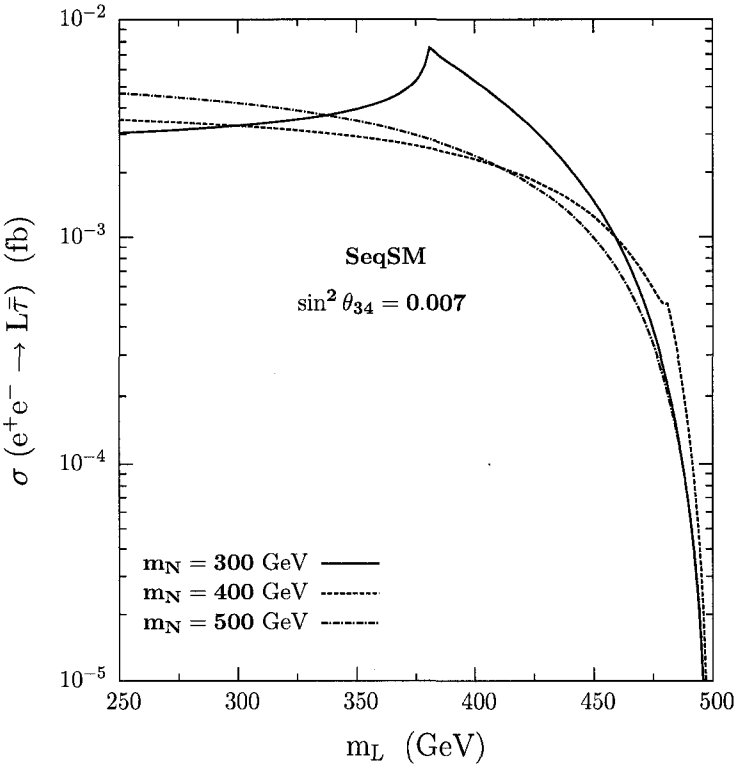

Figure 5.5: The total cross-section of $e^+e^- \to L\bar{\tau}$ as a function of the heavy lepton mass m_L for $\sqrt{s} = 500$ GeV and various heavy neutrino masses in an unpolarized electron-positron beam within the sequential SM framework.

`FormCalc`, and `LoopTools` packages [82, 83, 84, 85, 86]. We first patched the SM and 2HDM model files of the `FeynArts` package by introducing the fourth generation leptons and their interactions. Then, the numerical analysis was carried out in Fortran with the help of `FormCalc` and `LoopTools`. The cancellation of the ultraviolet and infrared divergences has been checked numerically and the expected cancellation was confirmed. In addition, as a separate check the expected null result for the cross-section due to unitarity of the mixing matrix V_{ij} was also tested numerically by setting the heavy neutrino mass m_N to

zero. Note that the same technique is applied for the calculation in the 2HDM, presented in the next section.

The results are plotted in Fig. 5.5 for neutrino masses of $300, 400$ and 500 GeV. We see that, for $\sin^2\theta_{34} = 0.007$, cross-sections of the order of a few attobarns can be expected. We can also show that as the neutrino mass increases, the cross-section grows rapidly, reaching 500 attobarns at $M_N = 2000$ GeV. This is not surprising since the theory is chiral. Of course, the cross-section scales with V_{34}; the value we have chosen is the maximum allowed from the analysis of Swain and Taylor [81].

The structure of the curves in Fig. 5.5 can be easily understood. Since the theory is chiral, one expects the cross-section to increase as the mass of the heavy neutrino m_N increases. However, as seen from Fig. 5.5, this is not necessarily true for neutrinos in the $300 - 400$ GeV mass range. One can understand, for example, why the the curve for $m_N = 300$ GeV crosses and becomes bigger than the one for $m_N = 400$ GeV and similar behavior occurs between the $m_N = 400$ GeV and $m_N = 500$ GeV curves. This is simply due to the fact that both the W boson and the heavy neutrino N go on-shell in the loop if the condition $m_L \geq m_W + m_N$ is kinematically satisfied. When m_L is large enough to produce the W and N on-shell, the loop integrals develop imaginary parts, which can be calculated by using the Cutkosky rules, and

results in enhancement of the cross-section. One can calculate this by cutting through the W boson-ν_i propagators (for $i = 4$) at the heavy lepton's leg in Fig. 5.4. Thus, for example, the peak due this enhancement for the $m_N = 300$ GeV curve occurs at around $m_N + m_W$ and it shifts to the right for the $m_N = 400$ GeV curve.

Are these small cross-sections detectable? With an integrated luminosity of an inverse attobarn, expected at the ILC's full luminosity for a couple of years, one expects a handful of events. The tau is monochromatic, and is opposite a monochromatic W and a light neutrino. We know of no backgrounds to this signature, and a complete analysis would be worthwhile.

5.2.2 The Two-Higgs Doublet and Randall-Sundrum Models

The Two-Higgs Doublet Model

The minimal Standard Model Higgs sector consists of one complex Higgs doublet. One of the simplest and most popular extensions of the Higgs sector is the two-Higgs doublet model (2HDM). By requiring that all fermions of a given electric charge couple to no more than one Higgs doublet [87], one avoids flavor changing neutral currents. This is accomplished with a simple Z_2 symmetry.

The 2HDM is an attractive model for several reasons:

- it contains charged Higgs bosons and pseudoscalars
- it adds relatively few new arbitrary parameters
- it allows for spontaneous CP violation, and can give sufficient baryogenesis
- this structure of the Higgs sector is required in low-energy supersymmetric models

A very detailed discussion of the 2HDM can be found in the Higgs Hunter's Guide [88].

This model has two complex, $Y = 1$, $SU(2)_L$ doublet scalar fields Φ_1 and Φ_2 where

$$\Phi_i = \begin{pmatrix} \phi_i^{\pm} \\ \\ \phi_i^0 \end{pmatrix} \tag{5.9}$$

for $i = 1, 2$. The vacuum expectation values of the neutral components of the Higgs doublets are v_1 and v_2, respectively. It is useful to define

$$\tan\beta = \frac{v_2}{v_1}. \tag{5.10}$$

The physical Higgs fields consist of two neutral scalars, a neutral pseudoscalar and a charged Higgs scalar. In the charged sector, there will be both a Goldstone boson and a physical Higgs state. The charged Higgs is a mixing of the

two new scalar fields ϕ_1 and ϕ_2 and is given by

$$H^{\pm} = -\phi_1^{\pm} \sin\beta + \phi_2^{\pm} \cos\beta \tag{5.11}$$

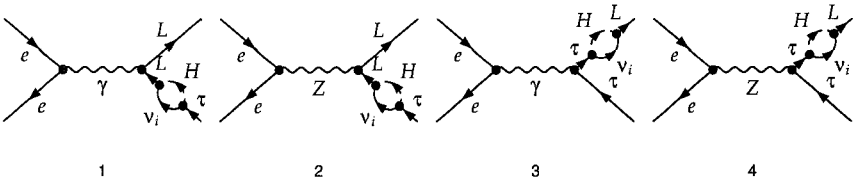

(a) The extra self energy diagrams in 2HDM.

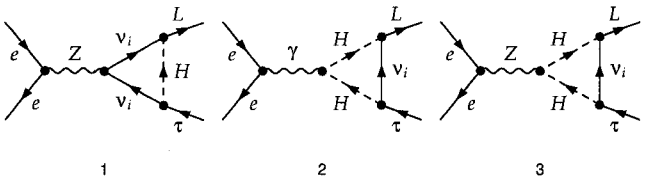

(b) The extra vertex diagrams in 2HDM.

Figure 5.6: Extra diagrams contributing to $e^+e^- \to L\bar{\tau}$ in 2HDM.

For our calculation, the neutral scalars will not contribute. However, the charged Higgs boson will contribute. One simply replaces the charged Goldstone boson, G in Fig. 5.4 with the charged Higgs boson; these diagrams are shown in Fig. 5.6. The only exception is that the $ZW^{\mp}H^{\pm}$ vertex vanishes [88]. There are now two new parameters in the calculation, the mass of the charged Higgs boson and $\tan\beta$.

There are two versions of the 2HDM. In Model I, all of the fermions couple to one of the Higgs doublets; in Model II (which is included in) supersymmetric

models, the neutral leptons couple to one doublet and the charged leptons couple to the other. The relevant Yukawa couplings are

$$\begin{aligned} L - N - H^+ \ : \quad & \frac{ie}{2\sqrt{2} m_W \sin\theta_W} \left[\frac{m_N}{\tan\beta}(1-\gamma_5) + m_L Y (1+\gamma_5) \right] \\ e_i - N - H^+ \ : \quad & \frac{-ie\delta_{i,3} V_{34}}{2\sqrt{2} m_W \sin\theta_W} \left[\frac{m_N}{\tan\beta}(1-\gamma_5) + m_{ei} Y (1+\gamma_5) \right] \\ L - \nu_i - H^+ \ : \quad & \frac{ie\delta_{i,3} V_{34}}{2\sqrt{2} m_W \sin\theta_W} m_L Y (1+\gamma_5) \end{aligned} \tag{5.12}$$

where $Y = -1/\tan\beta$ for Model I and $\tan\beta$ for Model II and the vertices for the ordinary lepton – ordinary neutrino – H^+ can be found in the Higgs Hunter's Guide [88].

Constraints from $b \to s\gamma$ force the mass of the charged Higgs to exceed approximately 200 GeV [89]. $\tan\beta$ and $\cot\beta$ must be less than about 3 so that the charged and neutral lepton Yukawa coupling remain perturbative.

The results are presented for Model I and for Model II in Fig. 5.7. We see small changes in the cross-section for $1 < \tan\beta < 3$, but substantial changes for $1 < \cot\beta < 3$. In both models, the cross-section can be enhanced by up to a factor of ten, leading to much easier detection at the ILC. Note that the vertices involving the heavy neutrino scales a $1/\tan\beta$, and thus the cross-section is enhanced if $\tan\beta < 1$ as seen from Fig. 5.7.

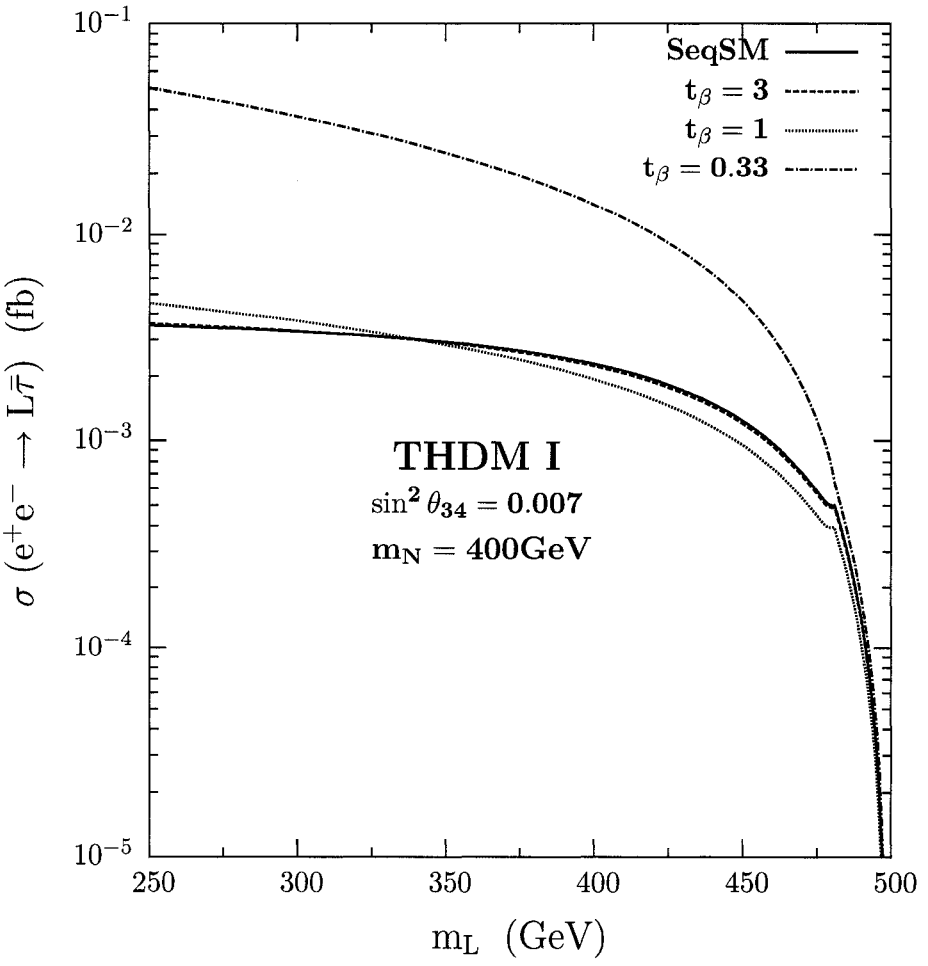

(a) Model I

Figure 5.7: The total cross-section of $e^+e^- \to L\bar{\tau}$ as a function of the heavy lepton mass m_L for $\sqrt{s} = 500$ GeV in an unpolarized electron-positron beam for various $\tan\beta$ values in 2HDM. In both graphs, the heavy neutrino and charged Higgs masses are set 400 GeV and 200 GeV, respectively.

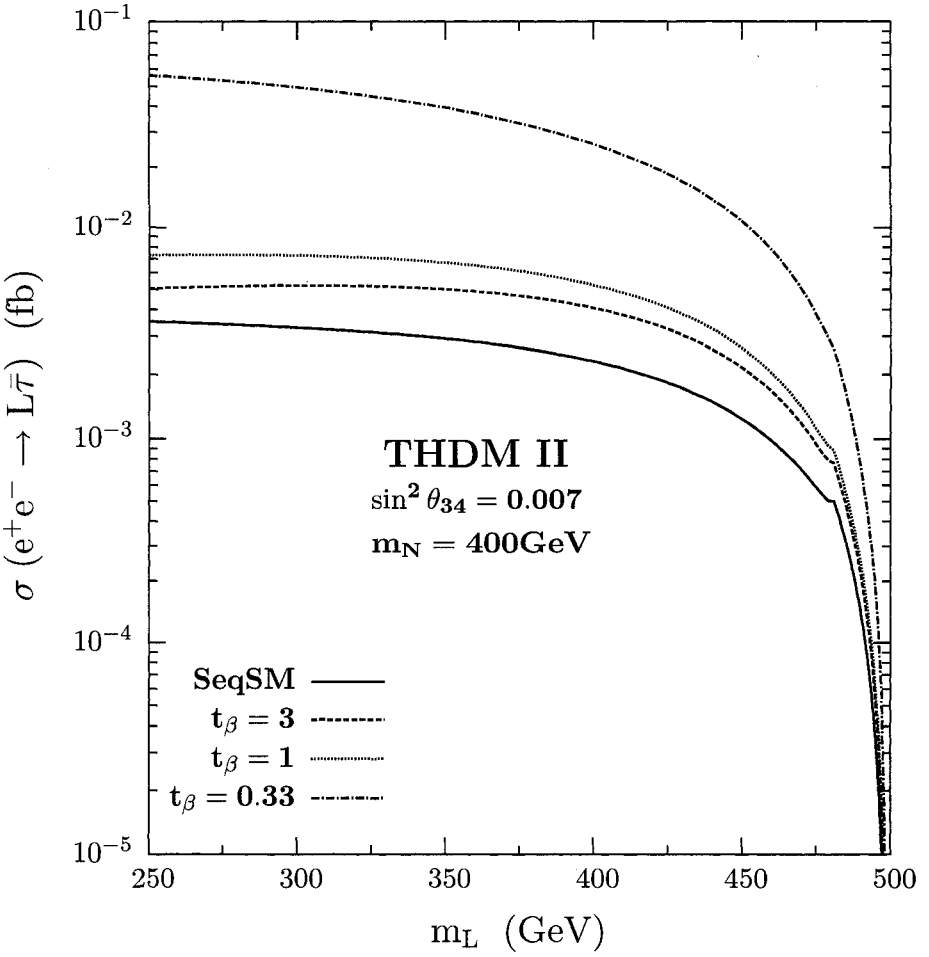

(b) Model II

Figure 5.7: The total cross-section of $e^+e^- \to L\bar{\tau}$ as a function of the heavy lepton mass m_L for $\sqrt{s} = 500$ GeV in an unpolarized electron-positron beam for various $\tan\beta$ values in 2HDM. In both graphs, the heavy neutrino and charged Higgs masses are set 400 GeV and 200 GeV, respectively.

The Randall-Sundrum Model

In its original formulation, the Randall-Sundrum model had all of the fermions on the TeV brane. More interesting phenomenology can occur when the Standard Model fermions and gauge bosons can propagate in the bulk [13, 18, 19]. In this case, the profiles of bulk fermion wavefunctions depend on their 5D mass parameters. By choosing the lighter fermions to live near the Planck brane, one can naturally explain the small Yukawa couplings for the light fermions, since their overlap with the TeV-brane localized Higgs boson is exponentially supressed. Thus the model can also explain the flavor hierarchy, since large differences in Yukawa couplings can arise from small differences in the mass parameters. The flavor hierarchy simply becomes a matter of geography in the fifth dimension.

In an interesting series of papers, Agashe, Perez and Soni [90, 91, 92] discussed the phenomenological implications of the flavor structure of these models. They noted that one expects larger flavor changing neutral currents for the heavier generations, thus evading bounds involving light quarks. In particular [92], Agashe, et al. considered top flavor violation at colliders, considering $t \to cZ$ at the LHC, and $e^+e^- \to t\bar{c}$ at the ILC. Clearly, a similar process could lead to $e^+e^- \to L\tau$ as well, if a fourth generation exists. The mechanism is caused by the fact that the couplings of the fermions to the gauge boson

Kaluza-Klein (KK) modes are not universal due to the different profiles for the fermions, and mixing between the gauge KK modes and the gauge bosons leads to flavor violating couplings of the Z. We refer the reader to Ref. [92] for details.

One can simply carry over the calculation of $e^+e^- \to t\bar{c}$ in Ref. [92] to this model. There is, however, one crucial difference. Since the couplings of the left-handed b quark to the Z are measured to an accuracy of less than one percent and the b quark is in a doublet with the left-handed top, one cannot put the left-handed top and bottom too close to the TeV brane. The right-handed top, however, can be close to the TeV brane. Thus the top flavor violation is predominantly right-handed. In the four generation case, there are no such restrictions, therefore the L flavor violation is relatively unconstrained. For definiteness, we choose the same magnitude for the left- and right-handed flavor violation, and set the coefficient of the $\bar{L}\gamma_\mu \tau Z^\mu$ term to be the same as that of the $\bar{t}_R \gamma_\mu c_R Z^\mu$ term in the Agashe, et al. analysis [92]. This is not unreasonable, since $m_c/m_t \sim m_\tau/m_L$ indicates that similar mixing angles may be expected.

Using this flavor violating coupling, one can find the total cross-section for $e^+e^- \to L\tau$. The result depends as well on the KK scale. It has been shown [64] that a custodial $SU(2)$ symmetry in the bulk can allow the KK gauge

boson mass to be as low as 3 TeV, and perhaps somewhat lower if a modest fine-tuning is allowed, without conflicting with precision electroweak results. Rather than calculate the interference with the Standard Model diagrams, we simply look at the RS model effects in isolation. This is because the uncertainty in the flavor-violating couplings preclude precise calculations. We find that if M_{KK} is 1 TeV, then the cross-section varies from 1.0 to 0.5 femtobarns as the L mass varies from 250 GeV to 350 GeV, and scales as $1/M_{KK}^4$. Thus, we see a significant enhancement of the cross-section in the KK mass range of $1-3$ TeV. One should keep in mind that the KK gauge bosons, if they exist, will be discovered at the LHC long before the ILC is constructed.

5.2.3 Detection and Conclusions

There are two possible decay modes for the L. It can decay into NW, or into $\nu_\tau W$. Of course, if the N is heavier only the latter decay is possible. Regardless, there will be substantial missing energy in the decay.

For the $e^+e^- \to L\tau$ process detection should be extremely straightforward, since the τ is monochromatic. For an L mass of 300 GeV, the τ energy is 160 GeV, leading to a decay length, γct, of 0.8 centimeters. This is comparable to the size of the inner vertex detector at the ILC.

In a wide region of the mass-mixing angle plane, the L will decay into a ν_τ

and a W. This would seem to give a clear signature, with a monochromatic τ, a monochromatic W and missing energy. The primary background will be from τ pairs, where one of the τ's is misidentified. A detailed Monte Carlo analysis is beyond the scope of this paper, but if the background can be eliminated, then a few events will suffice to discover the L.

In the Standard Model case, we have found that there will be a few events produced at the ILC, and the question of whether or not the L can be detected depends on the details of the detector and Monte Carlo simulations.

We then considered contributions from the charged Higgs boson of a 2HDM, as well as flavor changing effects in the Randall-Sundrum model. In both cases, there are regions of parameter space in which the cross-section is substantially higher, leading to straightforward detection at the ILC.

Long before the ILC is built, the LHC will have determined whether or not a fourth generation exists. If it does exist, then detection of the charged heavy lepton at the LHC will be very difficult and perhaps impossible. At the ILC, if the mass of the heavy lepton is more than half $\sqrt{s}$, pair production will be impossible, and the process calculated in this Chapter may be the only mechanism for detection.

Chapter 6

Conclusions

The LHC and ILC will provide copious data at higher energies. It is essential to determine the model that best describes nature. Thus we study how to discover and distinguish models at the colliders. We have studied two different models of extra dimensions and the addition of a fourth generation of matter.

In Chapter 3, we learned that it will not be possible to observe KK mesons. We will have to rely on KK quarkonium or other stable bound states to detect KK bound states in Universal Extra Dimensions.

Chapter 4 showed it will be possible to detect the effects of the KK particles up to 150 TeV for direct KK gauge boson exchange in top quark production in the Randall-Sundrum model of extra dimensions. This greatly extends the measurable parameter space for KK gauge bosons.

Detecting heavy charged leptons was discussed in Chapter 5. It is likely the

LHC will not be able to detect heavy leptons, but the there is strong chance to observe them at the ILC. Looking for single heavy lepton production allows the ILC to detect them for masses above 250 GeV.

Bibliography

[1] S. L. Glashow, Nucl. Phys. **22**, 579 (1961).

[2] S. Weinberg, Phys. Rev. Lett. **19**, 1264 (1967).

[3] A. Salam and J. C. Ward, Phys. Lett. **13**, 168 (1964).

[4] D. H. Perkins, *Introduction to High Energy Physics*, 4 ed. (Cambridge University Press, 2000).

[5] W. N. Cottingham and D. A. Greenwood, *An Introduction to the Standard Model of Particle Physics* (Cambridge University Press, 1998).

[6] T.-P. Cheng and L.-F. Li, *Gauge Theory of Elementary Particle Physics* (Oxford, 1983).

[7] W. M. Yao *et al.*, J. Phys. G **33**, 1 (2006).

[8] J. Davis, Raymond, D. S. Harmer, and K. C. Hoffman, Phys. Rev. Lett. **20**, 1205 (1968).

[9] SNO, Q. R. Ahmad *et al.*, Phys. Rev. Lett. **87**, 071301 (2001), nucl-ex/0106015.

[10] Super-Kamiokande, S. Fukuda *et al.*, Phys. Rev. Lett. **86**, 5651 (2001), hep-ex/0103032.

[11] M. W. Grunewald, (2007), arXiv:0710.2838 [hep-ex].

[12] L. Randall and R. Sundrum, Phys. Rev. Lett. **83**, 3370 (1999), hep-ph/9905221.

[13] A. Pomarol, Phys. Lett. **B486**, 153 (2000), hep-ph/9911294.

[14] H. Davoudiasl, J. L. Hewett, and T. G. Rizzo, Phys. Lett. **B473**, 43 (2000), hep-ph/9911262.

[15] S. J. Huber and Q. Shafi, Phys. Rev. **D63**, 045010 (2001), hep-ph/0005286.

[16] S. J. Huber, C.-A. Lee, and Q. Shafi, Phys. Lett. **B531**, 112 (2002), hep-ph/0111465.

[17] S. J. Huber, Nucl. Phys. **B666**, 269 (2003), hep-ph/0303183.

[18] T. Gherghetta and A. Pomarol, Nucl. Phys. **B586**, 141 (2000), hep-ph/0003129.

[19] Y. Grossman and M. Neubert, Phys. Lett. **B474**, 361 (2000), hep-ph/9912408.

[20] ALEPH, Phys. Rept. **427**, 257 (2006), hep-ex/0509008.

[21] P. H. Frampton, P. Q. Hung, and M. Sher, Phys. Rept. **330**, 263 (2000), hep-ph/9903387.

[22] F. del Aguila, M. Perez-Victoria, and J. Santiago, JHEP **09**, 011 (2000), hep-ph/0007316.

[23] J. E. Cieza Montalvo and M. D. Tonasse, Nucl. Phys. **B623**, 325 (2002), hep-ph/0008196.

[24] S. Nie and M. Sher, Phys. Rev. **D63**, 053001 (2001), hep-ph/0011077.

[25] A. Arhrib and W.-S. Hou, Phys. Rev. **D64**, 073016 (2001), hep-ph/0012027.

[26] H.-J. He, N. Polonsky, and S.-f. Su, Phys. Rev. **D64**, 053004 (2001), hep-ph/0102144.

[27] M. Maltoni, V. A. Novikov, L. B. Okun, A. N. Rozanov, and M. I. Vysotsky, Phys. Lett. **B476**, 107 (2000), hep-ph/9911535.

[28] V. A. Novikov, L. B. Okun, A. N. Rozanov, and M. I. Vysotsky, Phys. Lett. **B529**, 111 (2002), hep-ph/0111028.

[29] V. A. Novikov, L. B. Okun, A. N. Rozanov, and M. I. Vysotsky, JETP Lett. **76**, 127 (2002), hep-ph/0203132.

[30] G. D. Kribs, T. Plehn, M. Spannowsky, and T. M. P. Tait, Phys. Rev. **D76**, 075016 (2007), 0706.3718.

[31] ALEPH, J. Alcaraz *et al.*, (2006), hep-ex/0612034.

[32] E. Gates and J. Terning, Phys. Rev. Lett. **67**, 1840 (1991).

[33] B. A. Kniehl and H.-G. Kohrs, Phys. Rev. **D48**, 225 (1993).

[34] B. Holdom, JHEP **08**, 076 (2006), hep-ph/0606146.

[35] R. M. Barnett *et al.*, Snowmass summer study, 1988, p. 159.

[36] S. S. D. Willenbrock and D. A. Dicus, Phys. Lett. **B156**, 429 (1985).

[37] P. H. Frampton, D. Ng, M. Sher, and Y. Yuan, Phys. Rev. **D48**, 3128 (1993), hep-ph/9210270.

[38] H. Ciftci and S. Sultansoy, Mod. Phys. Lett. **A18**, 859 (2003), hep-ph/0107321.

[39] E. Arik *et al.*, Phys. Rev. **D58**, 117701 (1998).

[40] R. Ciftci, A. K. Ciftci, E. Recepoglu, and S. Sultansoy, Turk. J. Phys. **27**, 179 (2003), hep-ph/0203083.

[41] M. Drees and M. M. Nojiri, Phys. Rev. Lett. **72**, 2324 (1994), hep-ph/9310209.

[42] M. Drees and M. M. Nojiri, Phys. Rev. **D49**, 4595 (1994), hep-ph/9312213.

[43] M. Antonelli and N. Fabiano, Eur. Phys. J. **C16**, 361 (2000), hep-ph/9906535.

[44] U. Sarid and S. D. Thomas, Phys. Rev. Lett. **85**, 1178 (2000), hep-ph/9909349.

[45] C. D. Carone, J. M. Conroy, M. Sher, and I. Turan, Phys. Rev. **D69**, 074018 (2004), hep-ph/0312055.

[46] T. Appelquist, H.-C. Cheng, and B. A. Dobrescu, Phys. Rev. **D64**, 035002 (2001), hep-ph/0012100.

[47] H.-C. Cheng, K. T. Matchev, and M. Schmaltz, Phys. Rev. **D66**, 036005 (2002), hep-ph/0204342.

[48] V. D. Barger and R. J. N. Philips, *Collider Physics*, Frontiers in Physics Vol. 71 (Addison-Wesley, 1996).

[49] K. Monig, LC-PHSM-2000-060.

[50] G. Wilson, LC-PHSM-2001-009.

[51] C. Csaki, (2004), hep-ph/0404096.

[52] T. G. Rizzo, (2004), hep-ph/0409309.

[53] H. Davoudiasl, J. L. Hewett, and T. G. Rizzo, Phys. Rev. Lett. **84**, 2080 (2000), hep-ph/9909255.

[54] S. Chang, J. Hisano, H. Nakano, N. Okada, and M. Yamaguchi, Phys. Rev. **D62**, 084025 (2000), hep-ph/9912498.

[55] C. Csaki, J. Erlich, and J. Terning, Phys. Rev. **D66**, 064021 (2002), hep-ph/0203034.

[56] H. Georgi, A. K. Grant, and G. Hailu, Phys. Lett. **B506**, 207 (2001), hep-ph/0012379.

[57] M. S. Carena, T. M. P. Tait, and C. E. M. Wagner, Acta Phys. Polon. **B33**, 2355 (2002), hep-ph/0207056.

[58] H. Davoudiasl, J. L. Hewett, and T. G. Rizzo, Phys. Rev. **D68**, 045002 (2003), hep-ph/0212279.

[59] D. Dooling and K. Kang, Phys. Lett. **B502**, 189 (2001), hep-ph/0009307.

[60] H. Davoudiasl, J. L. Hewett, and T. G. Rizzo, Phys. Rev. **D63**, 075004 (2001), hep-ph/0006041.

[61] M. S. Carena, A. Delgado, E. Ponton, T. M. P. Tait, and C. E. M. Wagner, Phys. Rev. **D68**, 035010 (2003), hep-ph/0305188.

[62] M. S. Carena, A. Delgado, E. Ponton, T. M. P. Tait, and C. E. M. Wagner, Phys. Rev. **D71**, 015010 (2005), hep-ph/0410344.

[63] S. J. Huber and Q. Shafi, Phys. Lett. **B498**, 256 (2001), hep-ph/0010195.

[64] K. Agashe, A. Delgado, M. J. May, and R. Sundrum, JHEP **08**, 050 (2003), hep-ph/0308036.

[65] J. L. Hewett, F. J. Petriello, and T. G. Rizzo, JHEP **09**, 030 (2002), hep-ph/0203091.

[66] F. del Aguila, M. Perez-Victoria, and J. Santiago, Acta Phys. Polon. **B34**, 5511 (2003), hep-ph/0310353.

[67] F. del Aguila, M. Perez-Victoria, and J. Santiago, Eur. Phys. J. **C33**, s773 (2004), hep-ph/0310352.

[68] F. del Aguila, M. Perez-Victoria, and J. Santiago, JHEP **02**, 051 (2003), hep-th/0302023.

[69] G. Moreau and J. I. Silva-Marcos, JHEP **03**, 090 (2006), hep-ph/0602155.

[70] T. Appelquist, H.-C. Cheng, and B. A. Dobrescu, Phys. Rev. **D64**, 035002 (2001), hep-ph/0012100.

[71] S. Godfrey, (1996), hep-ph/9612384.

[72] American Linear Collider Working Group, T. Abe *et al.*, (2001), hep-ex/0106057.

[73] U. Baur, (2005), hep-ph/0508151.

[74] ECFA/DESY LC Physics Working Group, J. A. Aguilar-Saavedra *et al.*, (2001), hep-ph/0106315.

[75] A. Juste *et al.*, ECONF **C0508141**, PLEN0043 (2005), hep-ph/0601112.

[76] G. Cacciapaglia, C. Csaki, C. Grojean, and J. Terning, Phys. Rev. **D71**, 035015 (2005), hep-ph/0409126.

[77] B. C. Allanach *et al.*, (2006), hep-ph/0602198.

[78] E. Eichten, I. Hinchliffe, K. D. Lane, and C. Quigg, Rev. Mod. Phys. **56**, 579 (1984).

[79] I. Hinchliffe, Int. J. Mod. Phys. **A4**, 3867 (1989).

[80] J. I. Illana and T. Riemann, Phys. Rev. **D63**, 053004 (2001), hep-ph/0010193.

[81] J. Swain and L. Taylor, Phys. Rev. **D55**, 1 (1997), hep-ph/9610242.

[82] T. Hahn and M. Perez-Victoria, Comput. Phys. Commun. **118**, 153 (1999), hep-ph/9807565.

[83] T. Hahn, Nucl. Phys. Proc. Suppl. **89**, 231 (2000), hep-ph/0005029.

[84] T. Hahn, Comput. Phys. Commun. **140**, 418 (2001), hep-ph/0012260.

[85] T. Hahn and C. Schappacher, Comput. Phys. Commun. **143**, 54 (2002), hep-ph/0105349.

[86] T. Hahn, (2005), hep-ph/0506201.

[87] S. L. Glashow and S. Weinberg, Phys. Rev. **D15**, 1958 (1977).

[88] J. F. Gunion, H. E. Haber, G. Kane, and S. Dawson, *The Higgs Hunter's Guide*, Frontiers in Physics Vol. 80 (Addison-Wesley, 1990).

[89] F. Borzumati and A. Djouadi, Phys. Lett. **B549**, 170 (2002), hep-ph/9806301.

[90] K. Agashe, G. Perez, and A. Soni, Phys. Rev. Lett. **93**, 201804 (2004), hep-ph/0406101.

[91] K. Agashe, G. Perez, and A. Soni, Phys. Rev. **D71**, 016002 (2005), hep-ph/0408134.

[92] K. Agashe, G. Perez, and A. Soni, Phys. Rev. **D75**, 015002 (2007), hep-ph/0606293.

Vita
Erin Kathleen De Pree

Born in Redmond, Washington, a suburb of Seattle, to Paul and Kathy De Pree, Erin Kathleen De Pree has three younger sisters and one younger brother. De Pree always wanted to be a scientist since she was a small child. Familial lore contends that about the age of seven or eight, De Pree announced she would "go to grad school, become a professor, and be on boards and such."

Homeschooled since preschool, De Pree graduated high school in 1999. After her first year at Hillsdale College, De Pree worked as a physics tutor every Tuesday evening for the next three years. During her senior year, De Pree was honored with the Oustanding Physics Senior award. She also shared the Taylor Mathematics Prize with two other mathematics majors, all of whom had perfect 4.0 mathematics grade point averages. In 2003, De Pree received her Bachelors of Science in Physics and Mathematics, *summa cum laude*, Honors Program, with Honors in Mathematics from Hilllsdale.

In the fall of 2003, De Pree entered the graduate program in physics at the College of William and Mary. After passing the qualifying exam in August 2004, De Pree earned her Masters of Science in Physics from the College of William and Mary that December. During her graduate studies, De Pree attended the Theoretical Advanced Studies Institute at the University of Colorado at Boulder and the Hadron Collider Physics summer school at CERN, Geneva, Switzerland.

In August 2008, De Pree will become an Assistant Professor of Physics at St. Mary's College of Maryland.